Multi-Scale Modeling of Physical Phenomena: Adaptive Control of Models

J. Tinsley Oden,[1] Serge Prudhomme,[2] Albert Romkes,[3]
and Paul Bauman[4]

Institute for Computational Engineering and Sciences
The University of Texas at Austin
Austin, Texas 78712

Abstract

It is common knowledge that the accuracy with which computer simulations can depict physical events depends strongly on the choice of the mathematical model of the events. Perhaps less appreciated is the notion that the error due to modeling can be defined, estimated, and used adaptively to control modeling error, provided one accepts the existence of a base model that can serve as a datum with respect to which other models can be compared. In this work, it is shown that the idea of comparing models and controlling model error can be used to develop a general approach for multi-scale modeling, a subject of growing importance in computational science. *A posteriori* estimates of modeling error in so-called quantities of interest are derived and a class of adaptive modeling algorithms is presented. Generalizations of the theory to the problem of adaptive calibration of models are presented for cases in which experimental data on certain quantities of interest are available and the base model itself is not well defined. Several applications of the theory and methodology are presented. These include the analysis of molecular dynamics models using various techniques for scale bridging, molecular statics with applications to problems in nanoindentation in which errors generated by the quasicontinuum method are estimated and controlled. Other applications include very preliminary work on random multi-phase composite materials, modeling quantum mechanics, and the quantum mechanics-molecular dynamics interface.

Keywords: multi-scale modeling, goal-oriented adaptive modeling, *a posteriori* error estimation.

Contents

---

[1]Director of ICES and Cockrell Family Regents Chair of Engineering
[2]Research Scientist, ICES
[3]ICES Post Doctoral Fellow
[4]Graduate Research Assistant and DOE Fellow

1   Introduction

1.1   Introductory remarks

The development of mathematical and computational modeling techniques for simulating physical events that occur across several spatial and temporal scales has become one of the most challenging and important areas of computational science. Advances in nanotechnolgy, semiconductors, cell and molecular biology, biomedicine, geological and earth sciences, and many other areas hinge upon understanding the interactions of events at scales that could range from subatomic dimensions and nanoseconds to macroscales and hours or even centuries. Available computational methods have largely been designed to model events that take place over one, or rarely two spatial scales, and are generally nonapplicable to multi-scale phenomena. Molecular dynamics, for example, may provide an acceptable basis for modeling atomistic or molecular motions

2

over a time period on the order of nanoseconds, while nanodevice fabrications may involve events occurring over seconds or minutes.

In the present exposition, we develop a general approach to multi-scale modeling based on the notion of *a posteriori* estimation of modeling error and on adaptive modeling using so-called Goals algorithms. By a mathematical model we mean a collection of mathematical constructions – partial differential, integral, ordinary, or algebraic equations, boundary and initial conditions, constraints, and data – that provide an abstraction of a class of physical phenomena covered by scientific theory. Traditionally, a model is selected by a modeler, the analyst, who chooses a model, based on experience, or empirical evidence, heuristics, and personal judgment, to depict events assumed to involve well-defined spatial and temporal scales. Events at different scales require, in general, the use of different models. Thus, multi-scale models should generally involve a blending or adaptation of models of one scale of events with those of another. It would seem to follow, therefore, that successful multi-scale modeling techniques should be able to compare models of different structure and to adapt features of different models so that they deliver results of an accuracy sufficient to capture essential features of the response or to make engineering decisions. This is the basis for the methodologies developed in the present work.

This presentation reviews and extends the theory and methodology developed in earlier works (*e.g.* [32]) and extends the scope of applications to a broad range of problems, including problems in molecular statics, multiphase random materials, and to problems of model calibration and definition. The general tact is different from other techniques proposed in the rapidly-growing literature on multi-scale modeling.

Several surveys of the literature on multi-scale modeling have been published, and we mention in particular the articles of Liu *et al.* [26], E *et al.* [15], and Curtin and Miller [11]. In [26], it is asserted that multi-scale methods can be naturally grouped into two categories: concurrent and hierarchical. Concurrent methods simultaneously solve a fine-scale model in some local region of interest and a coarser scale model in the remainder of the domain. Hierarchical, or serial coupling methods [14], use results of a fine scale model simulation to acquire data for a coarser scale model that is used globally, *e.g.* to determine parameters for constitutive equations. The methodologies we develop here are more akin to concurrent approaches since the notion of adaptive modeling fits naturally within that framework. Additionally, the various applications we present here are largely described in terms of problems in mechanics and materials science, although the framework is very general and is applicable to multi-scale problems in virtually all areas of science.

We identify three main thrusts in the current literature for implementing multi-scale methods. The first involves dimensional reduction approaches such as that used by Tadmor, Ortiz, and Phillips in the quasicontinuum method (QCM) [53, 55]. The QCM has been applied to quasi-static fracture [27, 30], grain-boundary interaction [48], and nanoindentation [54, 52]. In these applications, the QCM has led to a dramatic reduction in the number of degrees of freedom while still resolving physical features of interest.

A second line of research in concurrent multi-scale methods is the decomposition-of-scales technique used by Liu *et al.* in the bridging-scale method [60, 40, 56, 57].

3

The scale decomposition provides a natural separation of spatial and temporal scales for coupling molecular dynamics and continuum models and has successfully reduced spurious wave reflection in preliminary tests. A static formulation has been applied to the deformation of carbon nanotubes in [43], and a three-dimensional generalization to problems in dynamic fracture is presented in [39].

Finally, perhaps the most widely used scheme in concurrent methods is directly interfacing an atomistic and continuum model using "pad", "overlap", or "hand-shake" regions. The first method to use such schemes was the FEAt method [25], which was used to simulate the fracture of b.c.c. crystals using a molecular and continuum model. The FEAt method later provided the foundations of the well-known molecular, atomistic, *ab initio* dynamics (MAAD) or coupling of length scales (CLS) method [10], which was the first to concurrently couple quantum, molecular, and continuum scales. The atomistic-continuum interface in the MAAD method was extended by Belytschko and Xiao with the bridging-domain method [7, 61] by using an augmented Lagrange method to enforce displacement boundary conditions in the overlap region as well as separating temporal scales in the numerical implementation. The coupled atomistic and discrete dislocation plasticity (CADD) method [50] was developed by Shilkrot, Miller, and Curtin to interface an atomistic model, similar to the QCM, with a more complex continuum model that incorporates descriptions for dislocation movement [58]. In this way, dislocations can be passed to the continuum model, or vice-versa, thereby preserving degrees of freedom that would otherwise be needed to track the dislocation movement. Published implementations of the CADD method are two-dimensional and static, although work in developing three-dimensional and dynamic models is reportedly underway [51].

There also exist more general schemes that develop modeling frameworks rather than concentrating on the details of model interfaces. The heterogeneous multiscale method (HMM) [13], proposed by E and Engquist, provides such a framework for designing multi-scale methods based upon the particular nature of the problem. The HMM has been applied to many mathematical problems that possess solutions with multiple scales, see e.g. [14], and some work has been done in *a priori* error estimation for elliptic problems [16].

The idea of estimating modeling error and controling error through model adaptivity was inspired by work on *a posteriori* estimation of numerical approximation error and control of error through adaptive meshing [1, 31, 5]. Oden, Zohdi, and co-workers [63, 38, 37] used global error estimates to drive adaptivity of models of multi-phase heterogeneous elastic materials. Upper and lower bounds of modeling errors in local quantities of interest for this class of problems were presented in [36] and model adaptivity based on the Goals algorithm was first presented in [59]. Further extensions of these approaches are described in [45, 33] and a general theory for model error estimation is proposed in [32].

In the remainder of this introduction, we review the basic ideas behind our error estimation methodology and the Goals algorithm for adaptive modeling, and we lay down notations and assumptions prerequisite to subsequent developments. The basic theorems on model error estimation are taken up in Section 2. Discussions of some technicalities connected with ensemble averaging and homogenization are given

in Section 3. Section 4 describes extensions to cases in which the data are unknown or random and in which results of experimental tests are available. The Goals algorithms are discussed in Section 5. There we describe two general versions of these types of algorithms that have proved to be very effective in several application areas. A brief account of global error estimates is given in Section 6. Applications are discussed in Section 7, and conclusions are collected in a final section.

1.2 Basic ideas

The basic idea behind the multi-scale modeling approach to be described here is one of computing and controling modeling error. We first assume that we can define a general mathematical model of a physical system which can serve as a datum with respect to which other models can be compared. This *fine* or *base* model may be highly complex, even intractable, it may involve incomplete data, and, in general, it is never "solved". In studying multi-scale phenomena, this base model will depict events that take place on the finest (smallest) spatial and temporal scales. An abstract setting for many base models is embodied in the problem:

$$\text{Find } u \in V \text{ such that } A(u) = F \text{ in } V'$$

where V is an appropriate topological vector space, $A(\cdot)$ is a nonlinear operator mapping V into its dual, V', and F is given data in V'. If $\langle \cdot, \cdot \rangle$ denotes duality pairing on $V' \times V$, then the above problem is equivalent to

$$\boxed{\begin{aligned} &\text{Find } u \in V \text{ such that} \\ &\quad B(u;v) = F(v), \quad \forall v \in V \end{aligned}} \tag{1}$$

where

$$B(u;v) = \langle A(u), v \rangle, \quad F(v) = \langle F, v \rangle \tag{2}$$

the semi-colon signaling that $B(\cdot;\cdot)$ may be a nonlinear function of the argument u to the left of the semi-colon, but linear in the test vector v to the right of it.

Now, in all applications of interest, we do not merely want to characterize the vectors u satisfying (1), but rather we want to find a particular physical event or feature of the system that depends upon u. Such *quantities of interest* are characterized by functionals Q of the solutions to (1). Thus, our actual target problem is this:

$$\boxed{\begin{aligned} &\textit{If } u \textit{ is a solution of (1), find } Q(u), \textit{ where } Q : V \to \mathbb{R} \\ &\textit{is a given functional defining a quantity of interest.} \end{aligned}} \tag{3}$$

If (1) is intractable, so is (3). We must therefore seek an approximation to $Q(u)$.

Let u_0 be an arbitrary member of V. In the case that the forms $B(\cdot;\cdot)$ and $Q(\cdot)$ are sufficiently smooth (twice differentiable in a certain functional sense), it is shown in [32] that the error

$$\varepsilon = Q(u) - Q(u_0) \tag{4}$$

coincides with the sum of a *residual functional*,

$$\mathcal{R}(u_0, p) = F(p) - B(u_0; p) \tag{5}$$

p being the solution of an appropriately defined dual or adjoint problem, and higher order terms involving the error $e_0 = u - u_0$. We examine this result in more detail in Section 2.

An important observation is that the trial solution u_0 may itself be the solution of some other *surrogate* mathematical model, characterized by a different semilinear form $B_0(\cdot; \cdot)$ and linear form $F_0(\cdot)$; i.e. u_0 is then the solution of the problem,

$$\text{Find } u_0 \in V: \quad B_0(u_0; v) = F_0(v), \quad \forall v \in V \tag{6}$$

Thus, the fact that the error between the quantity of interest $Q(\cdot)$ computed using the base model (1) and that computed using any other surrogate model (6) can be estimated in some manner, provides a means for comparing the appropriateness of different models and, presumably, controlling modeling error relative to the base model. The surrogate problem(s) (6) will therefore correspond to models of coarser (larger) scales than (1). Still, the base model may never be solved; it remains a datum with respect to which various surrogates are measured.

1.3 Adaptive modeling

If modeling error can be effectively estimated, the next challenge is to adaptively control it by systematically changing the surrogate models. This is the goal of the Goals algorithms: to adapt the mathematical model so that preset tolerances in the error in the specific quantity of interest can be met. Here we will describe a general family of algorithms that include earlier methods as special cases (see [36, 59]). The surrogate model that can approximate the base model well enough to lead to a small tolerable error may often be a hybrid consisting of components involving several different spatial or temporal scales. We take this subject up in Section 5.

1.4 Notation: functional derivatives and Taylor formulas

We define the functional or Gâteaux derivative of the semilinear form $B(u; v)$ in (1) as

$$B'(u; w, v) = \lim_{\theta \to 0} \theta^{-1}[B(u + \theta w; v) - B(u; v)]$$

assuming this limit exists. Higher derivatives of $B(u; v)$ are defined analogously:

$$B''(u; w_1, w_2, v) = \lim_{\theta \to 0} \theta^{-1}[B'(u + \theta w_2; w_1, v) - B'(u; w_1, v)]$$
$$B'''(u; w_1, w_2, w_3, v) = \lim_{\theta \to 0} \theta^{-1}[B''(u + \theta w_3; w_1, w_2, v) - B''(u; w_1, w_2, v)]$$
$$\vdots$$

Thus, for each $u \in V$, $B'(u; w, v)$ is a bilinear form in v and w, $B''(u; w_1, w_2, v)$ is a trilinear form in w_1, w_2, and v, $B'''(u; w_1, w_2, w_3, v)$ is a quadrilinear form in w_1, w_2,

w_3, v; etc. Similarly, if the target output functionals (the quantities of interest Q) are differentiable, we use the following notations for various Gâteaux derivatives:

$$Q'(u; v_1) = \lim_{\theta \to 0} \theta^{-1}[Q(u + \theta v_1) - Q(u)]$$

$$Q''(u; v_1, v_2) = \lim_{\theta \to 0} \theta^{-1}[Q'(u + \theta v_2; v_1) - Q'(u; v_1)]$$

$$Q'''(u; v_1, v_2, v_3) = \lim_{\theta \to 0} \theta^{-1}[Q''(u + \theta v_3; v_1, v_2) - Q''(u; v_1, v_2)]$$

$$\vdots$$

Taylor formulas with integral remainders can easily be constructed for such differentiable functionals and semilinear forms. Among many such expansions, we list as examples the following:

$$Q(u + v) - Q(u) = \int_0^1 Q'(u + sv; v)ds$$

$$Q(u + v) - Q(u) = Q'(u; v) + \int_0^1 Q''(u + sv; v, v)(1 - s)ds$$

$$Q(u + v) - Q(u) = \frac{1}{2}Q'(u; v) + \frac{1}{2}Q'(u + v; v)$$

$$+ \frac{1}{2}\int_0^1 Q'''(u + sv; v, v, v)(s - 1)s \ ds$$

and

$$B(u + w; v) - B(u; v) = \int_0^1 B'(u + sw; w, v)ds$$

$$B(u + w; v) - B(u; v) = B'(u; w, v) + \int_0^1 B''(u + sw; w, w, v)(1 - s)ds$$

We shall say that $B(\cdot; \cdot)$ and $Q(\cdot)$ belong to $C^r(V)$ whenever the limits defining functional derivatives of order r exist. Partial functional derivatives may also be defined; e.g., if $J(u, v) : V \times V \to \mathbb{R}$ and $J(u, v)$ is nonlinear in u and v, we write

$$J_u(u, v; w) = \lim_{\theta \to 0} \theta^{-1}[J(u + \theta w, v) - J(u, v)]$$

$$J_v(u, v; w) = \lim_{\theta \to 0} \theta^{-1}[J(u, v + \theta w) - J(u, v)]$$

etc. whenever these limits exist. In all of the theory and applications we consider in subsequent sections, V is a reflexive Banach space with norm $\|\cdot\|$. The theory can be extended to more general settings.

2   *A Posteriori* Estimates of Modeling Error

We begin with the observation that the target problem (3) can be viewed as a problem of optimal control: find an extremum of Q subject to the constraint (1):

$$Q(u) = \inf_{v \in M} Q(v); \quad M = \{w \in V; \ B(w; q) = F(q), \quad \forall q \in V\} \tag{7}$$

The Lagrangian associated with (7) is

$$L(v, q) = Q(v) + F(q) - B(v; q) \tag{8}$$

and, assuming Q and B are Gâteaux differentiable, solutions to the constrained optimization problem (7) are pairs (u, p) such that

$$L'((u, p); (v, q)) = 0, \quad \forall (v, q) \in V \times V$$

i.e. (u, p) is a solution of the coupled problem,

$$
\boxed{
\begin{aligned}
&\text{Find } (u, p) \in V \times V \text{ such that}\\
&\qquad B(u; q) \;=\; F(q), \qquad \forall q \in V\\
&\qquad B'(u; v, p) \;=\; Q'(u; v), \qquad \forall v \in V
\end{aligned}
}
\tag{9}
$$

We refer to $(9)_1$ as the *primal* base problem and to $(9)_2$ as the *dual* base problem. The dual problem is thus always linear in p. The dual solution p is called the *influence vector* (or *function*) or the *generalized Green's function*. In the cases in which $B(\cdot; \cdot)$ is a bilinear form and $Q(\cdot)$ is a linear functional, the dual problem $(9)_2$ reduces to

$$B(v, p) = Q(v), \quad \forall v \in V$$

so that

$$Q(u) = B(u, p) = F(p). \tag{10}$$

This is recognized as a generalization of the property of Green's functions for linear initial- and boundary-value problems.

Now let us suppose that the system (9) is intractable and that we seek an approximation (u_0, p_0) to (u, p). The following theorem provides the error in the quantity of interest Q:

Theorem 1 ([32]) *Let the semilinear form $B(\cdot; \cdot)$ in (9) belong to $C^3(V)$ and let the quantity of interest $Q(\cdot) \in C^1(V)$. Let $(u, p) \in V \times V$ be a solution of the base problem (9) and let (u_0, p_0) be an arbitrary pair in $V \times V$. Then the error in $Q(u)$ produced by u_0 is given by*

$$\mathcal{E}(u_0) = Q(u) - Q(u_0) = \mathcal{R}(u_0; p_0) + \mathcal{R}(u_0; \varepsilon_0) + \Delta_1(u_0, p_0, e_0, \varepsilon_0) \tag{11}$$

where $\mathcal{R}(u_0; v)$ is the residual functional,

$$\mathcal{R}(u_0; v) = F(v) - B(u_0; v), \quad v \in V \tag{12}$$

and $\Delta_1 = \Delta_1(u_0, p_0, e_0, \varepsilon_0)$ is the remainder,

$$
\begin{aligned}
\Delta_1 = \;& \frac{1}{2} \int_0^1 \{ B''(u_0 + se_0; e_0, e_0, p_0 + s\varepsilon_0) \\
& \qquad\qquad - Q''(u_0 + se_0; e_0, e_0) \} ds \\
& + \frac{1}{2} \int_0^1 \{ Q'''(u_0 + se_0; e_0, e_0) - 3B''(u_0 + se_0; e_0, e_0, \varepsilon_0) \\
& \qquad\qquad - B'''(u_0 + se_0; e_0, e_0, e_0, p_0 + s\varepsilon_0) \}(s-1)s\,ds
\end{aligned}
\tag{13}
$$

8

with

$$e_0 = u - u_0 \ \text{and} \ \varepsilon_0 = p - p_0. \tag{14}$$

$\square$

We observe that $\Delta_1 \equiv 0$ whenever $B(\cdot; \cdot)$ is bilinear and $Q(\cdot)$ is linear. In that case, $Q(u) - Q(u_0) = \mathcal{R}(u_0; p_0) + \mathcal{R}(u_0; \varepsilon_0) = \mathcal{R}(u_0; p_0) + B(e_0, \varepsilon_0)$. Equation (11) establishes that the error $\mathcal{E}(u_0)$ is dominated by the residual functional evaluated at the influence functional p_0 to within terms of higher order in the error components (14).

An alternative representation of the error $\mathcal{E}(u_0)$, involving the residuals associated with the primal and dual problems in given in the following corollary.

Corollary 1 ([32]) *Let the assumptions of Theorem 1 hold. Then the error in $Q(u)$ produced by u_0 is given by*

$$\mathcal{E}(u_0) = \mathcal{R}(u_0; p_0) + \frac{1}{2}(\mathcal{R}(u_0; \varepsilon_0) + \bar{\mathcal{R}}(u_0, p_0; e_0)) + \Delta_2(u_0, p_0, e_0, \varepsilon_0) \tag{15}$$

where $\bar{\mathcal{R}}(u_0, p_0; v)$ is the residual functional for the dual problem:

$$\bar{\mathcal{R}}(u_0, p_0; v) = Q'(u_0; v) - B'(u_0; v, p_0), \quad v \in V \tag{16}$$

and $\Delta_2 = \Delta_2(u_0, p_0, e_0, \varepsilon_0)$ is given by:

$$\begin{aligned}
\Delta_2 = &\frac{1}{2} \int_0^1 \{Q'''(u_0 + se_0; e_0, e_0) - 3B''(u_0 + se_0; e_0, e_0, \varepsilon_0) \\
&- B'''(u_0 + se_0; e_0, e_0, e_0, p_0 + s\varepsilon_0)\}(s-1)s\,ds.
\end{aligned} \tag{17}$$

$\square$

We note that the remainder in (17) should be smaller in practical applications than the one in (11) at the expense of having to determine or estimate both e_0 and ε_0. Results similar to those in Theorem 1 and Corollary 1 for finite element approximation errors were presented in Oden and Prudhomme [31] and Becker and Rannacher [5]. A detailed account of the versions of the methods of [5] is given in [4].

It is emphasized that the surrogate functions (u_0, p_0) in (11)–(14) are completely arbitrary vectors in $V \times V$. However, the most natural choice of these vectors are those which are solutions of a *surrogate problem* of the form

$$\boxed{\begin{aligned}
&\text{Find } (u_0, p_0) \in V \times V \text{ such that} \\
&\quad B_0(u_0; v) \ = \ F_0(v), \quad\quad \forall\, v \in V \\
&\quad B_0'(u_0; v, p_0) \ = \ Q_0'(u_0; v), \quad \forall\, v \in V
\end{aligned}} \tag{18}$$

where $B_0(\cdot; \cdot)$ is a semilinear form for a coarser-scale problem and $F_0(\cdot)$ and $Q_0(\cdot)$ are coarse-scale approximations of $F(\cdot)$ and $Q(\cdot)$. In most cases, B_0, F_0, and Q_0 are obtained through an appropriate homogenization or averaging process. Thus, (18) could represent models of events that occur at scales larger than those of the base model. Theorem 1 then provides a means for comparing models of different scales.

3 Homogenization and Construction of Surrogates

3.1 Some general remarks

Symbolically, one can envision a multi-scale model in which the quantity of interest $Q(u)$ of the base model is the target output, $Q(u_1)$ is the approximation of that output produced by a coarser-scale model obtained through a homogenization process, $Q(u_2)$ is the approximation due to a still-coarser scale, and so on. If u_N denotes the surrogate solution to the coarsest scale model, the various modeling error components are:

$$Q(u) - Q(u_N) = \underbrace{Q(u) - Q(u_1)}_{\text{error in scale 1 model}} + \underbrace{Q(u_1) - Q(u_2)}_{\substack{\text{error in scale 2 model} \\ \text{relative to scale 1}}}$$

$$+ \underbrace{Q(u_2) - Q(u_3)}_{\substack{\text{error in scale 3 model} \\ \text{relative to scale 2}}} + \ldots + \underbrace{Q(u_{N-1}) - Q(u_N)}_{\substack{\text{error in scale } N \text{ model} \\ \text{relative to scale } N-1}}$$

Each error component, of course, depends upon how the successive coarser models are obtained through a homogenization process. The scenario is illustrated symbolically in Fig. 1. As will be seen in applications discussed later, if a target error level is specified, the models that can ultimately deliver that accuracy may involve a mosaic of component models of several different scales.

We also note that the rigor of methods of homogenization can vary, with a very rough averaging process often the only connection between models of different scales. In some cases, the term homogenization is not at all descriptive of the process of coarsening scales. For instance, in embedding quantum mechanics models into a molecular dynamics setting, we may call upon the Bohr correspondence principle to justify Newtonian mechanics models without defining a meaningful limiting process. We comment further on this topic in Section 7.

It can be argued that the limit processes carrying models of one scale to those of larger scales, such as the limiting process from molecular models to continuum models, is a central problem to the mathematical foundations of multi-scale modeling. It is a subject in which some progress has been made in recent years (see *e.g.* [8, 19]), but for which much additional work remains to be done. It is a remarkable fact, however, that even when these processes are not understood and when only crude averaging procedures are employed, the adaptive modeling algorithms described later may still produce acceptable results, albeit at slow rates of convergence.

Finally, we note that in all applications we are only able to compute a numerical approximation u_0^h of any particular surrogate problem solution u_0. However, we can write

$$\underbrace{Q(u) - Q(u_0^h)}_{\text{total error}} = \underbrace{Q(u) - Q(u_0)}_{\text{modeling error}} + \underbrace{Q(u_0) - Q(u_0^h)}_{\text{approximation error}}$$

The total error $Q(u) - Q(u_0^h)$ can be estimated with the aid of Theorem 1 using u_0^h instead of u_0. The approximation error $Q(u_0) - Q(u_0^h)$ can be accurately estimated and controlled using the theory and methodology discussed in [31] (see also [1, 5, 4, 35]).

Finally, an estimate of the modeling error is obtained by substracting the approximation error from the total error.
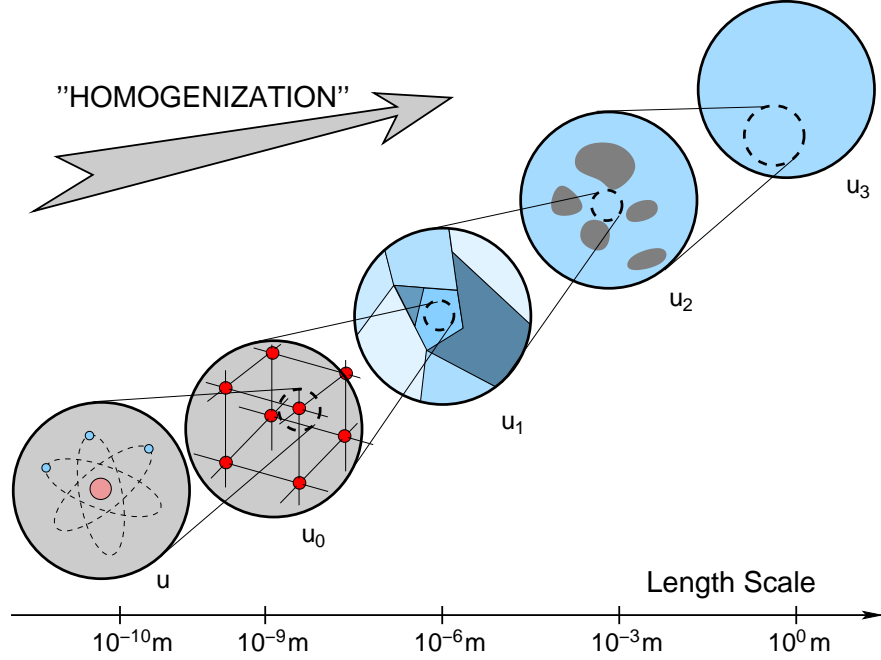

Figure 1: Hierarchy of models and scales. Not all transitions to coarser scales are simple homogenizations.

It should be understood that while models involving an ascending sequence of scales can, in theory, be obtained through some sort of ensemble averaging (homogenization) process, as suggested in Fig. 1, the actual surrogate pairs (u_0, p_0) appearing in the error estimate (11) are not necessarily solutions of a homogenized problem defined for coarser scale models. In fact, the coarse-scale models obtained through homogenization processes may even belong to different function spaces than those appearing in the base problem. For example, if the base model is discrete, such as is the case in which the base model corresponds to a crystalline lattice model or a molecular dynamics model, and a homogenization process produces a continuum model, then the continuum model cannot be used as the surrogate within the context of our theory. Another step is needed.

Let the following denote a model obtained from the base model through some homogenization:

$$(\tilde{u}, \tilde{p}) \in V_0 \times V_0 :$$
$$\tilde{B}(\tilde{u}; \tilde{v}) = \tilde{F}(\tilde{v}), \qquad \forall \tilde{v} \in V_0$$
$$\tilde{B}'(\tilde{u}; \tilde{v}, \tilde{p}) = \tilde{Q}'(\tilde{u}; \tilde{v}), \qquad \forall \tilde{v} \in V_0$$

where $\tilde{B}(\cdot; \cdot)$, $\tilde{F}(\cdot)$, and $\tilde{Q}(\cdot)$ are functionals produced from $B(\cdot, \cdot)$, $F(\cdot)$, and $Q(\cdot)$ through homogenization. Let $\Pi(\cdot)$ denote a map,

$$\Pi : V_0 \longrightarrow V; \quad \Pi\tilde{u} = u_0, \ \Pi\tilde{p} = p_0.$$

11

Then, for any appropriate choice of Π, we use (u_0, p_0) as the solutions of the surrogate models, and the error in the quantity of interest is estimated with respect to $Q(u_0)$. We provide examples of such surrogates in Section 7.

3.2 Fine-scale fluctuations about a mean

Various methods for treating the interactions of events at two or more scales begin with the separation of the fine scale solution u into a "mean" component $\bar{u}$ and a fluctuation u' about the mean (see, *e.g.* [56, 57])

$$u = \bar{u} + u' \tag{19}$$

Comparing to our notation, if $V_0 \subset V$, the component $\bar{u}$ and u' can be identified with u_0 and $e_0 = u - u_0$ as:

$$\bar{u} = u_0 \quad \text{and} \quad u' = e_0 \tag{20}$$

Using the developments laid down thus far, it is a straightforward exercise to determine approximate relationships for coarse-scale/fine-scale interactions and for computing the fluctuations.

Ignoring higher-order terms in the component u' (assumed small compared to $\bar{u}$), we have, for any $v \in V$

$$F(v) = B(\bar{u} + u'; v) \approx B(\bar{u}; v) + B'(\bar{u}; u', v)$$

Thus

$$\boxed{B'(\bar{u}; u', v) \approx \mathcal{R}(\bar{u}; v), \qquad \forall v \in V} \tag{21}$$

That is, the fluctuations u' satisfy the transpose of the dual problem with u replaced by $\bar{u}$ and with $q'(u; v)$ replaced by the residual functional $\mathcal{R}(\bar{u}; v)$. Then, with p the solution of the corresponding primal dual problem,

$$\boxed{B'(\bar{u}; u', p) \approx \mathcal{R}(\bar{u}; p) \approx Q(u) - Q(\bar{u})} \tag{22}$$

The result establishes a relationship between the fine-scale fluctuations u' and the error $\mathcal{E}(\bar{u})$ in the quantity of interest. The fine-scale fluctuations thus affect the error in the quantity of interest at positions of the space-time domain within the support of the dual solution p.

At the heart of many multi-scale methods is the particular homogenization strategy used to compute the mean component $\bar{u}$. if $\Pi : V_0 \to V$ is a given extension of the space containing the surrogate solution such that $\Pi u_0 = \bar{u}$, then one can construct the "filter", $Pu = \bar{u}$ so that the fluctuations $u - Pu = u'$ are minimized in some sense. We described one such approach in Section 7.

4 Relationship to Calibration of Models

Recent work on calibration of models and on inverse problems and optimization can be cast naturally into the general framework developed up to this point. In the present

context, we have in mind the calibration of models of physical phenomena as well as numerical approximations of surrogates. Our development displaces our initial work reported in an earlier edition [34] and parallels and extends the recent contribution of Becker and Vexler [6], Bangerth [3], and Johannson and Runesson [24] to problems of modeling calibration, error, and adaptivity. We here consider cases in which the characterization of the base model involves the specification of input data which are described by a function $\beta \in \mathbb{D}$, where $\mathbb{D}$ is a space with norm $\|\cdot\|_{\mathbb{D}}$. We shall regard β as a parameter function defining the coefficients appearing in the operators in the governing equations and boundary conditions, but more general cases could be considered. To indicate the dependence of the semilinear form on such coefficients, we rewrite the base problem as follows:

$$
\boxed{
\begin{aligned}
&\text{Find } u = u(\beta) \in V \text{ such that} \\
&\qquad B(\beta, u; v) = F(v), \quad \forall v \in V
\end{aligned}
}
\tag{23}
$$

We are interested in situations in which the following conditions prevail:

1. The coefficients β are unknown or known only approximately. But a surrogate model of (23) can be formulated using an initial guess or estimate $\beta_0 \in \mathbb{D}_0 \subset \mathbb{D}$ of β, leading to a tractable form $B(\beta_0, \cdot; \cdot)$.

2. Available are N experimental values $\{z^i\}_{i=1}^N$ that correspond to measurable features of the response $\{T^i(u(\beta))\}_{i=1}^N$, $T^i \colon V \longrightarrow \mathbb{R}$.

3. The goal of the computation is to predict a target quantity of interest $Q(u(\beta))$ that has not been measured by means of physical experiments.

In problems of *parameter identification* (*e.g.* see [3, 24]), the goal is to find the parameter function β characterizing a base model best fitting the experimental data set $\{z^i\}_{i=1}^N$, with $N \geq \dim(\mathbb{D})$. Toward this purpose, we introduce a *calibration functional*, *e.g.*

$$
C(\gamma, v) = \frac{1}{2} \sum_{i=1}^N (T^i(v(\gamma)) - z^i)^2 + \frac{c}{2} \|\gamma - \beta_0\|_{\mathbb{D}}^2, \qquad c > 0,
\tag{24}
$$

and state the problem of parameter identification in terms of the following constrained optimization problem:

$$
\begin{aligned}
&\text{Find } (\beta, u) \in \mathbb{D} \times V \text{ such that} \\
&\qquad C(\beta, u) = \inf_{(\gamma, v) \in M} C(\gamma, v) \\
&\qquad M = \left\{ (\gamma, v) \in \mathbb{D} \times V : \ B(\gamma, v; w) = F(w), \ \forall w \in V \right\}.
\end{aligned}
\tag{25}
$$

We assume that the solution to this problem exists and is unique (due to the regularization term in the calibration functional). The corresponding Lagrangian is

$$
A(\gamma, v, q) = C(\gamma, v) + F(q) - B(\gamma, v; q)
\tag{26}
$$

and the critical points (β, u, p) of A satisfy

$$A'((\beta, u, p); (\gamma, v, q)) = 0, \qquad \forall (\gamma, v, q) \in \mathcal{D} \times V \times V, \tag{27}$$

where

$$
\begin{aligned}
A'((\beta, u, p); (\gamma, v, q)) = & F(q) - B(\beta, u; q) \\
& + C_u(\beta, u; v) - B_u(\beta, u; v, p) \\
& + C_\beta(\beta, u; \gamma) - B_\beta(\beta, u; p, \gamma)
\end{aligned}
\tag{28}
$$

However, our focus here is on the problem of *model calibration,* where the goal is to use the experimental data to determine a model providing reliable predictions of a target quantity $Q(u(\beta))$. We assume here that no experimental data are available for this target quantity. Nevertheless, the accuracy in its prediction should meet user-defined error tolerances. Hence, the appropriate target problem is the following extension of (3):

$$\boxed{\textit{Find } Q(u(\beta)) \textit{ where } (\beta, u) \textit{ is a solution of the minimization problem (25)}}$$

We can therefore state an equivalent constrained minimization formulation (see also Section 2):

$$
\boxed{
\begin{aligned}
& \text{Find } (\beta, u) \in \mathbb{D} \times V \text{ such that} \\
& Q(u(\beta)) = \inf_{(\gamma, v) \in M^*} Q(v(\gamma)) \\
& M^* = \left\{ (\gamma, v) \in \mathbb{D} \times V : C(\gamma, v) = \inf_{(\varphi, w) \in M} C(\varphi, w) \right\}
\end{aligned}
}
\tag{29}
$$

where M^* obviously contains the solution to (27). The corresponding Lagrangian is

$$L((\gamma, v, q), (\varphi, w, r)) = Q(v(\gamma)) + A'((\gamma, v, q); (\varphi, w, r)) \tag{30}$$

Let $\mathcal{V} = \mathcal{D} \times V \times V$ and let the critical points of L be denoted by $\phi = (\beta, u, p)$ and $\theta = (\gamma, v, q)$. Then these points satisfy the equations:

$$L'((\phi, \theta); (\xi, \eta)) = L_\phi(\phi, \theta; \xi) + L_\theta(\phi, \theta; \eta) = 0, \qquad \forall (\xi, \eta) \in \mathcal{V}$$

which leads to a set of six equations governing the solutions (β, u, p) and (γ, v, q) of the calibration base problem,

$$
L_\theta(\phi, \theta; \eta) = 0 \quad \Leftrightarrow \quad
\boxed{
\begin{aligned}
B_\beta(\beta, u; p, \varphi) &= C_\beta(\beta, u; \varphi), & \forall \varphi \in \mathbb{D} \\
B_u(\beta, u; w, p) &= C_u(\beta, u; w), & \forall w \in V \\
B(\beta, u; r) &= F(r), & \forall r \in V
\end{aligned}
}
\tag{31}
$$

14

$$L_\phi(\phi, \theta; \xi) = 0 \iff \begin{array}{l} B_{\beta\beta}(\beta, u; p, \gamma, \chi) + B_{u\beta}(\beta, u; p, v, \chi) + B_\beta(\beta, u; q, \chi) \\[4pt] \quad = C_{u\beta}(\beta, u; v, \chi) + C_{\beta\beta}(\beta, u; \gamma, \chi) + Q_\beta(u(\beta); \chi), \\[4pt] \hfill \forall \chi \in \mathbb{D} \\[4pt] B_{\beta u}(\beta, u; p, \gamma, z) + B_{uu}(\beta, u; p, v, z) + B_u(\beta, u; q, z) \\[4pt] \quad = C_{uu}(\beta, u; v, z) + C_{\beta u}(\beta, u; \gamma, z) + Q_u(u(\beta); z), \\[4pt] \hfill \forall z \in V \\[4pt] B_\beta(\beta, u; s, \gamma) = -B_u(\beta, u; s, v), \hfill \forall s \in V \end{array} \tag{32}$$

We note that (32) can be simplified by substituting the last expression into the two previous equations,

$$\begin{aligned} B_\beta(\beta, u; q, \chi) &= C_{u\beta}(\beta, u; v, \chi) + C_{\beta\beta}(\beta, u; \gamma, \chi) + Q_\beta(u(\beta); \chi), &\forall \chi \in \mathbb{D} \\ B_u(\beta, u; q, z) &= C_{uu}(\beta, u; v, z) + C_{\beta u}(\beta, u; \gamma, z) + Q_u(u(\beta); z), &\forall z \in V \\ B_\beta(\beta, u; s, \gamma) &= -B_u(\beta, u; s, v), &\forall s \in V \end{aligned} \tag{33}$$

Systems (31) and (32) are generally untractable with current computational resources, so we aim at developing simpler models. For example, we may consider approximations (β_1, u_1, p_1) and (γ_1, v_1, q_1) of (β, u, p) and (γ, v, q) that are solutions to the surrogate problem,

$$\begin{aligned} B_\beta(\beta_1, u_1; p_1, \varphi) &= C_\beta(\beta_1, u_1; \varphi), &\forall \varphi \in \mathbb{D}_1 \\ B_u(\beta_1, u_1; w, p_1) &= C_u(\beta_1, u_1; w), &\forall w \in V \\ B(\beta_1, u_1; r) &= F(r), &\forall r \in V \\ B_\beta(\beta_1, u_1; q_1, \chi) &= C_{u\beta}(\beta_1, u_1; v_1, \chi) \\ &\quad + C_{\beta\beta}(\beta_1, u_1; \gamma_1, \chi) + Q_\beta(u_1(\beta_1); \chi), &\forall \chi \in \mathbb{D}_1 \\ B_u(\beta_1, u_1; q_1, z) &= C_{uu}(\beta_1, u_1; v_1, z) \\ &\quad + C_{\beta u}(\beta_1, u_1; \gamma_1, z) + Q_u(u_1(\beta_1); z), &\forall z \in V \\ B_\beta(\beta_1, u_1; s, \gamma_1) &= -B_u(\beta_1, u_1; s, v_1), &\forall s \in V \end{aligned} \tag{34}$$

where $\mathbb{D}_1$ is a suitable subspace of $\mathbb{D}$. The error of such solutions in the target quantity $Q(u(\beta))$ is given in the following theorem.

Theorem 2 *Let the forms $Q(\cdot)$ and $B(\cdot, \cdot; \cdot)$ be differentiable and let (β, u, p) and (γ, v, q) be solutions of (31) and (32), respectively. Let (β_1, u_1, p_1) and (γ_1, v_1, q_1) be arbitrary triples in $\mathbb{D} \times V \times V$ and let $e_\beta = \beta - \beta_1$, $e_u = u - u_1$, $e_p = p - p_1$, $e_\gamma = \gamma - \gamma_1$, $e_v = v - v_1$, and $e_q = q - q_1$. Then the error η in the quantity of interest*

$$\eta = Q(u(\beta)) - Q(u_1(\beta_1))$$

is given by

$$\begin{aligned} \eta =\ & A'((\beta_1, u_1, p_1); (\gamma_1, v_1, p_1)) \\ & + Q_\beta(u_1; e_\beta) + A'((\beta_1, u_1, p_1); (e_\gamma, e_v, e_q)) \\ & + Q_u(u_1; e_u) + A'_{\beta up}((\beta_1, u_1, p_1); (\gamma_1, v_1, q_1), (e_\beta, e_u, e_p)) + \Delta R, \end{aligned} \tag{35}$$

15

where $A'(\cdot;\cdot)$ is as defined in (28) and

$$
\begin{aligned}
A'_{\beta up}&((\beta_1, u_1, p_1); (\gamma_1, v_1, q_1), (e_\beta, e_u, e_p)) \\
&= C_{u\beta}(\beta_1, u_1; v_1, e_\beta) + C_{\beta\beta}(\beta_1, u_1; \gamma_1, e_\beta) \\
&\quad - B_{\beta\beta}(\beta_1, u_1; p_1, \gamma_1, e_\beta) - B_{u\beta}(\beta_1, u_1; p_1, v_1, e_\beta) \\
&\quad - B_\beta(\beta_1, u_1; q_1, e_\beta) + C_{uu}(\beta_1, u_1; v_1, e_u) \\
&\quad - B_{\beta u}(\beta_1, u_1; p_1, \gamma_1, e_u) + C_{\beta u}(\beta_1, u_1; \gamma_1, e_u) \\
&\quad - B_{uu}(\beta_1, u_1; p_1, v_1, e_u) - B_u(\beta_1, u_1; q_1, e_u) \\
&\quad - B_u(\beta_1, u_1; e_p, v_1) - B_\beta(\beta_1, u_1; e_p, \gamma_1),
\end{aligned}
\tag{36}
$$

$$
\begin{aligned}
\Delta R = \frac{1}{2}\int_0^1 L'''\Big(&((\beta_1, u_1, p_1), (\gamma_1, v_1, q_1)) + s((e_\beta, e_u, e_p), (e_\gamma, e_v, e_q)); \\
&((e_\beta, e_u, e_p), (e_\gamma, e_v, e_q)), ((e_\beta, e_u, e_p), (e_\gamma, e_v, e_q)), \\
&((e_\beta, e_u, e_p), (e_\gamma, e_v, e_q)) \Big) s(s-1)\mathrm{d}s.
\end{aligned}
\tag{37}
$$

Proof: The proof is a straightforward generalization of that of Theorem 1 in [32]. From the definition of the Lagrangian (30), we have

$$
\begin{aligned}
L((\beta, u, p), (\gamma, v, q)) &- L((\beta_1, u_1, p_1), (\gamma_1, v_1, q_1)) \\
&= Q(u(\beta)) - Q(u_(\beta_1) - A'((\beta_1, u_1, p_1); (\gamma_1, v_1, p_1))
\end{aligned}
$$

so that

$$
\eta = A'((\beta_1, u_1, p_1); (\gamma_1, v_1, p_1)) + L((\beta, u, p), (\gamma, v, q)) - L((\beta_1, u_1, p_1), (\gamma_1, v_1, q_1))
$$

To simplify notations, let ϕ, θ, ϕ_1, and θ_1 denote (β, u, p), (γ, v, q), (β_1, u_1, p_1), and (γ_1, v_1, q_1), respectively, and let $\Delta_\phi = \phi - \phi_1$ and $\Delta_\theta = \theta - \theta_1$. Then making use of one of the Taylor expansions, the difference between the Lagrangian terms becomes

$$
\begin{aligned}
L(\phi, \theta) - L(\phi_1, \theta_1)) &= \frac{1}{2}L'((\phi_1, \theta_1); (\Delta_\phi, \Delta_\theta)) + \frac{1}{2}L'((\phi, \theta); (\Delta_\phi, \Delta_\theta)) \\
&\quad + \frac{1}{2}\int_0^1 L'''((\phi_1, \theta_1) + s(\Delta_\phi, \Delta_\theta); (\Delta_\phi, \Delta_\theta), (\Delta_\phi, \Delta_\theta), (\Delta_\phi, \Delta_\theta))s(s-1)\mathrm{d}s
\end{aligned}
$$

The term $L'((\phi, \theta); (E_1, \Delta_\theta))$ simply vanishes since (ϕ, θ) defines a saddle point of the Lagrangian L. On the other hand, we have

$$
L'((\phi_1, \theta_1); (\Delta_\phi, \Delta_\theta)) = \underbrace{L_\phi(\phi_1, \theta_1; \Delta_\phi)}_{Q_\phi(\phi_1; \Delta_\phi) + A'_\phi(\phi_1; \theta_1, \Delta_\phi)} + \underbrace{L_\theta(\phi_1, \theta_1; \Delta_\theta)}_{A'(\phi_1; \Delta_\theta)}
$$

16

where

$$A'(\phi_1; \Delta_\theta) = F(q - q_1) - B(\beta_1, u_1; q - q_1) + C_u(\beta_1, u_1; v - v_1)$$
$$- B_u(\beta_1, u_1; v - v_1, p_1) + C_\beta(\beta_1, u_1; \gamma - \gamma_1)$$
$$- B_\beta(\beta_1, u_1; p_1, \gamma - \gamma_1)$$

$$Q_\phi(\phi_1; \Delta_\phi) = Q_u(u_1; u - u_1) + Q_\beta(u_1; \beta - \beta_1)$$

$$A'_\phi(\phi_1; \theta_1, \Delta_\phi) = C_{u\beta}(\beta_1, u_1; v_1, \beta - \beta_1) + C_{\beta\beta}(\beta_1, u_1; \gamma_1, \beta - \beta_1)$$
$$- B_{\beta\beta}(\beta_1, u_1; p_1, \gamma_1, \beta - \beta_1) - B_{u\beta}(\beta_1, u_1; p_1, v_1, \beta - \beta_1)$$
$$- B_\beta(\beta_1, u_1; q_1, \beta - \beta_1) + C_{uu}(\beta_1, u_1; v_1, u - u_1)$$
$$+ C_{\beta u}(\beta_1, u_1; \gamma_1, u - u_1) - B_{\beta u}(\beta_1, u_1; p_1, \gamma_1, u - u_1)$$
$$- B_{uu}(\beta_1, u_1; p_1, v_1, u - u_1) - B_u(\beta_1, u_1; q_1, u - u_1)$$
$$- B_u(\beta_1, u_1; p - p_1, v_1) - B_\beta(\beta_1, u_1; p - p_1, \gamma_1)$$

Finally, the remainder is:

$$\Delta R = \frac{1}{2} \int_0^1 L'''((\phi_1, \theta_1) + s(\Delta_\phi, \Delta_\theta); (\Delta_\phi, \Delta_\theta), (\Delta_\phi, \Delta_\theta), (\Delta_\phi, \Delta_\theta))s(s - 1)\mathrm{d}s$$

which confirms the assertion. $\square$

Corollary 2 *If (β_1, u_1, p_1) and (γ_1, v_1, q_1) are the solutions of the surrogate calibration problem (34), then the expression for the error in the quantity of interest simplifies to:*

$$\eta = Q_\beta(u_1; e_\beta) + C_{u\beta}(\beta_1, u_1; v_1, e_\beta) + C_{\beta\beta}(\beta_1, u_1; \gamma_1, e_\beta)$$
$$- B_{\beta\beta}(\beta_1, u_1; p_1, \gamma_1, e_\beta) - B_{u\beta}(\beta_1, u_1; p_1, v_1, e_\beta) - B_\beta(\beta_1, u_1; q_1, e_\beta) \qquad (38)$$
$$+ C_\beta(\beta_1, u_1; e_\gamma) - B_\beta(\beta_1, u_1; p_1, e_\gamma) + \Delta R.$$

Proof: If (β_1, u_1, p_1) are solutions of $(34)^{1,2,3}$, then by recalling (28) we observe that

$$A'((\beta_1, u_1, p_1); (\gamma, v, q)) = 0, \qquad \forall(\gamma, v, q) \in \mathcal{D}_1 \times V \times V.$$

Hence, (35) reduces to

$$\eta = Q_\beta(u_1; e_\beta) + A'((\beta_1, u_1, p_1); (e_\gamma, e_v, e_q)),$$
$$+ Q_u(u_1; e_u) + A'_{\beta up}((\beta_1, u_1, p_1); (\gamma_1, v_1, q_1), (e_\beta, e_u, e_p)) + \Delta R.$$

If in addition (γ_1, v_1, q_1) are solutions of $(34)^{4,5,6}$, we can similarly simplify the remaining terms, *i.e.*

$$A'((\beta_1, u_1, p_1); (e_\gamma, e_v, e_q)) = \underbrace{F(q - e) - B(\beta_1, u_1; e_q)}_{= 0, \text{ (see } (34)^3)}$$
$$+ \underbrace{C_u(\beta_1, u_1; e_v) - B_u(\beta_1, u_1; e_v, p_1)}_{= 0, \text{ (see } (34)^2)}$$
$$+ C_\beta(\beta_1, u_1; e_\gamma) - B_\beta(\beta_1, u_1; p_1, e_\gamma)$$

17

$$Q_\beta(u_1; e_\beta) + Q_u(u_1; e_u) + A'_{\beta up}((\beta_1, u_1, p_1); (\gamma_1, v_1, q_1), (e_\beta, e_u, e_p))$$

$$= Q_\beta(u_1; e_\beta) + C_{u\beta}(\beta_1, u_1; v_1, e_\beta) + C_{\beta\beta}(\beta_1, u_1; \gamma_1, e_\beta)$$

$$- B_{\beta\beta}(\beta_1, u_1; p_1, \gamma_1, e_\beta) - B_{u\beta}(\beta_1, u_1; p_1, v_1, e_\beta) - B_\beta(\beta_1, u_1; q_1, e_\beta)$$

$$+ \Big\{ C_{uu}(\beta_1, u_1; v_1, e_u) + C_{\beta u}(\beta_1, u_1; \gamma_1, e_u) - B_u(\beta_1, u_1; q_1, e_u)$$

$$+ Q_u(u_1; e_u) - B_{uu}(\beta_1, u_1; p_1, v_1, e_u) - B_{\beta u}(\beta_1, u_1; p_1, \gamma_1, e_u) \Big\}_{= 0, \, (\text{see } (34)^5)}$$

$$- \Big\{ B_u(\beta_1, u_1; e_p, v_1) + B_\beta(\beta_1, u_1; e_p, \gamma_1) \Big\}_{= 0, \, (\text{see } (34)^6)}$$

$$\square$$

Theorem 2 and Corollary 2 extend the theory presented in Section 2 to cases in which the base model is imperfectly or incompletely specified, but for which some observational data is assumed to be known. Adaptive modeling algorithms, such as that described in the next section, can be used to update a sequence of surrogate models until the coefficients and the model lead to an estimated error within preset tolerances.

Remark 1 *A few remarks are in order:*

1. *It is clear that the choice of the calibration functional given in (24) is but one of many possible choices. Any convex differentiable functional of the error components $T^i(\beta)) - z^i$ or $\beta - \beta_0$ can be used with no changes in the resulting form (35) of the error estimate.*

2. *The results are also immediately extendable to cases in which one considers a series of loadings, each delivering a different value z_j^i of features T^i. We then define the calibration functional as*

$$C(\beta, u) = \frac{1}{2} \sum_i \sum_j (T^i(u_j(\beta) - z_j^i)^2 + \frac{c}{2}\|\beta - \beta_0\|_{\mathbb{D}}^2.$$

$$\square$$

5   The Goals Algorithms

The Goals algorithms, introduced in [36, 59] and implemented in various versions in [33, 45, 46], are designed to reduce estimated modeling error by systematically adapting the model using a sequence of surrogates. In [36], reference is made to the "Goal-Oriented Adaptive Local Solutions" algorithms; hence "Goals". We refer to these general algorithms as Goals or goal-oriented algorithms. As will be shown, not all employ "local" solutions.

The general ideas can be described in the following setting:

1. Let the domain of the solution $(u, p) \in V \times V$ of the base problem (9) be an open region $D \subset \mathbb{R}^d$, and let $\{\Theta_j\}_{j=0}^k$ be a partition of D:

$$\overline{D} = \bigcup_{j=0}^k \overline{\Theta}_j, \quad \Theta_i \bigcap \Theta_j = \delta_{ij}, \quad 0 \le i, j \le k$$

The semilinear and linear forms in (9) can be broken into $k+1$ components so that

$$B(u; v) = \sum_{j=0}^k B_{\Theta_j}(u; v), \quad F(v) = \sum_{j=0}^k F_{\Theta_j}(v) \tag{39}$$

for u, $v \in V$, with $B_{\Theta_j}(\cdot; \cdot)$, $F_{\Theta_j}(\cdot)$ being the values of the forms produced by restrictions of u and v to Θ_j.

2. Next, through an averaging or homogenization process, we construct a surrogate problem of the form (18) and compute the surrogate solutions $(u_0, p_0) \in V \times V$ defined over all of D.

3. To assess the accuracy of the surrogate solution, we seek to estimate the modeling error in the quantity of interest and call upon Theorem 1 to note that to within higher order terms,

$$\mathcal{E}(u_0) \approx \mathcal{R}(u_0, p) = \mathcal{R}(u_0; p_0) + \mathcal{R}(u_0; p - p_0). \tag{40}$$

The first term is computable whereas the remaining term is generally intractable and has to be estimated. However, the derivation of an estimate depends heavily on the type of problem that is analyzed. Examples of error estimates for problems in molecular statics, elastostatics, and elastodynamics are given in [33, 36, 46, 45].

4. If the error estimate is to within a user defined error tolerance δ_{TOL}, the analysis stops and provides the analyst with the prediction of the quantity of interest $Q(u_0)$.

5. If the error exceeds the tolerance, the algorithm proceeds by enhancing or improving the surrogate model in a subdomain $D_L \subset D$, called the *domain of influence*. Suppose that the quantity of interest Q involves features of the solution confined to a subdomain $D_Q \subset D$ (*e.g.* $Q(u)$ could be the average of u or its derivatives over D_Q). Then the initial choice of D_L is generally the union of subdomains Θ_i that intersect with D_Q.

6. There are several possibilities to then compute a correction $(\tilde{u}, \tilde{p})$ of (u_0, p_0) using the enhanced surrogate model,

   I. **Global Goals Algorithms.** Let

   $$\tilde{B}(\tilde{u}; v) = B_{D_L}(\tilde{u}_{D_L}; v_{D_L}) + B_{0, D \backslash D_L}(\tilde{u}_{D \backslash D_L}; v_{D \backslash D_L}) \tag{41}$$

   where $\tilde{u}_{D_L} = \tilde{u}|_{D_L}$, *etc.* and $B_{0, D \backslash D_L}(\cdot; \cdot)$ is the semilinear form for the surrogate problem defined on restrictions of functions in V to $D \backslash D_L$. Thus,
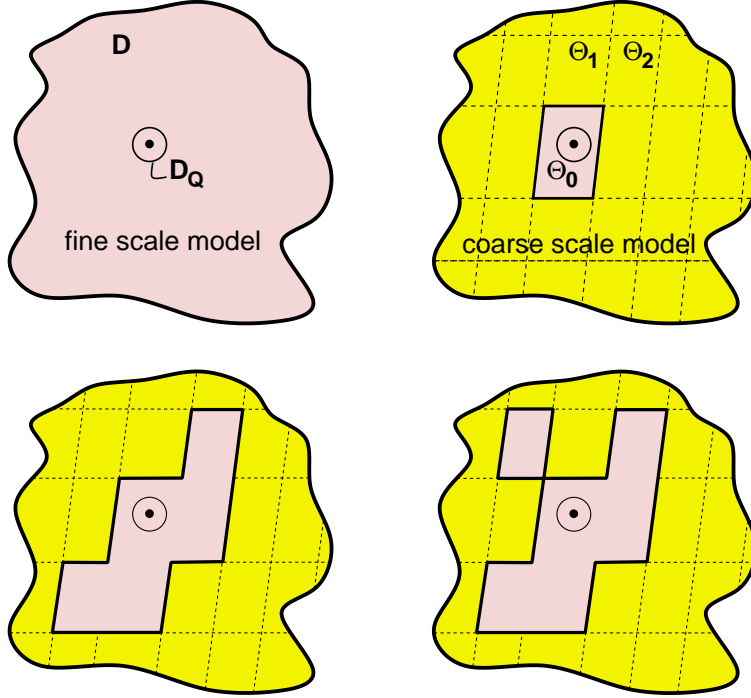
Figure 2: (top left) A fine scale base model and a subdomain ω_Q surrounding features of a quantity of interest Q; (top right) a partition of Ω into subdomains with an initial domain of influence $D = \Theta_0$; (bottom) successive enlargements of D designed to reduce the modeling error.

$\tilde{B}(\cdot, \cdot)$ includes fine-scale features of the base model over domain D_L while it is characterized by coarse-scale features of the surrogate model over $D \backslash D_L$. We calculate $(\tilde{u}, \tilde{p}) \in V \times V$ such that

$$\begin{aligned} \tilde{B}(\tilde{u}; v) &= F(v), \quad \forall v \in V \\ \tilde{B}'(\tilde{u}; v, \tilde{p}) &= Q'(\tilde{u}; v), \quad \forall v \in V \end{aligned} \tag{42}$$

II. **Local Goals Algorithms.** In this case, we compute a correction $(\tilde{u}, \tilde{p})$ that coincides with (u_0, p_0) outside the initial domain of influence, but uses the base problem data (the "fine scale data") within D_L:

$$\begin{aligned} B_{D_L}(\tilde{u}; v) &= F_{D_L}(v), \quad \forall v \in V(D_L) \quad \text{with} \quad \tilde{u} = u_0 \text{ in } \overline{D} \backslash D_L \\ B'_{D_L}(\tilde{u}; v, \tilde{p}) &= Q'_{D_L}(\tilde{u}; v), \quad \forall v \in V(D_L) \quad \text{with} \quad \tilde{p} = p_0 \text{ in } \overline{D} \backslash D_L \end{aligned} \tag{43}$$

and $V(D_L)$ is the space of restrictions of functions in V to the domain of influence D_L. The situation is illustrated in Fig. 2.

7. As done in step 3, we can derive an estimate of the modeling error of the enhanced solution $\tilde{u}$,

$$\mathcal{E}(\tilde{u}) \approx \mathcal{R}(\tilde{u}; p)$$

20

Again, the estimation of this term depends on the type of problem (*e.g.* see [36, 45]). In this work, we introduce an alternative estimator by noting that:

$$\mathcal{E}(\tilde{u}) = Q(u) - Q(\tilde{u}) = [Q(u) - Q(u_0)] + [Q(u_0) - Q(\tilde{u})] \qquad (44)$$

The last term in this equation is computable and the first can be estimated by again using Theorem 1,

$$\begin{aligned} \mathcal{E}(\tilde{u}) \ &\approx \mathcal{R}(u_0; p) + Q(u_0) - Q(\tilde{u}) \\ &= \mathcal{R}(u_0; \tilde{p}) + \mathcal{R}(u_0; p - \tilde{p}) + Q(u_0) - Q(\tilde{u}) \qquad (45) \\ &\approx \mathcal{R}(u_0; \tilde{p}) + Q(u_0) - Q(\tilde{u}) \end{aligned}$$

8. If the error estimate is to within a user defined error tolerance δ_{TOL}, the analysis stops and provides the analyst with the prediction in the quantity of interest $Q(\tilde{u})$.

9. If the error exceeds the tolerance, we obtain an indication of the error contribution of each subdomain (outside the domain of influence) by computing its contribution to the upper bound of the residual $\mathcal{R}(u_0; p)$ (*e.g.* see [36, 45, 46]). We then expand the domain of influence D_L by adding the subdomains $\{\Theta_i\}$ whose error contributions, with respect to the maximal contribution, exceed a user defined tolerance γ and return to step 6.

Steps 1- 9 characterize a family of Global and Local Goals algorithms for adaptive modeling. Several remarks are in order.

Remark 2 *While the global versions of the Goals algorithms may involve the solution of surrogate problems of a larger size that the local solution algorithms, they have the advantage of accounting for possible interactions of fine-scale and large-scale behavior. Thus, we expect that they may lead to faster convergence rates that the simpler local methods.* □

Remark 3 *The Local and Global Goals algorithms described suggest numerous alternative schemes, many of which may be similar to classical Schwartz schemes for domain decomposition.* □

Remark 4 *The initial domain of interest, of course, can be a multi-connected domain, depending upon the number and structure of the quantities of interest.* □

Remark 5 *The surrogate solutions (u_0, p_0), $(\tilde{u}, \tilde{p})$ are rarely (virtually never) known exactly, but $Q(u_0)$ and $Q(\tilde{u})$ can be replaced by numerical approximations $Q(u_0^h)$, $Q(\tilde{u}^h)$ and, for instance in (44),*

$$Q(u) - Q(\tilde{u}^h) = Q(u) - Q(u_0^h) + Q(u_0^h) - Q(\tilde{u}^h)$$

The approximation errors $Q(u_0) - Q(u_0^h)$ and $Q(\tilde{u}) - Q(\tilde{u}^h)$ can be estimated and controlled by established a posteriori error estimation techniques (see e.g. [31, 5]). □

6 Global Estimates

Global estimates of modeling error can be obtained for specific forms of $B(\cdot;\cdot)$ and $Q(\cdot)$. In cases in which $B(\cdot;\cdot)$ is a symmetric, positive-definite, bilinear form, global estimates of e_0 $(= u - u_0)$ and ε_0 $(= p - p_0)$ can be used to construct upper and lower bounds of errors in quantities of interest [36, 59, 45]. Here we provide a derivation of such bounds for cases in which $B(\cdot;\cdot)$ and $Q(\cdot)$ satisfy a priori conditions.

Let V be a Banach space with norm $\|\cdot\|$. We observe that

$$B(u + w; v) = B(u; v) + B'(u; w, v) + \Delta_4(u, w, v)$$
$$Q'(u + w; v) = Q'(u; v) + \Delta_5(u, w, v)$$
$$B'(u + w_2; w_1, v) = B'(u; w_1, v) + \Delta_6(u, w_1, w_2, v)$$

where

$$\Delta_4(u, w, v) = \int_0^1 B''(u + sw; w, w, v)(1 - s)ds$$

$$\Delta_5(u, w, v) = \int_0^1 Q''(u + sw; w, v)ds$$

$$\Delta_6(u, w_1, w_2, v) = \int_0^1 B''(u + sw_2; w_1, w_2, v)ds$$

for all u, v, w, w_1, and w_2 in V. With this notation, and recalling that $u = u_0 + e_0$ and $p = p_0 + \varepsilon_0$, we have

$$\left.\begin{array}{l} B(u; v) = B(u_0; v) + B'(u_0; e_0, v) + \Delta_4(u_0, e_0, v) \\ Q'(u; v) = Q'(u_0; v) + \Delta_5(u_0, e_0, v) \\ B'(u; v, p) = B'(u_0; v, p_0) + B'(u_0; v, \varepsilon_0) + \Delta_6(u_0, v, e_0, p_0 + \varepsilon_0) \end{array}\right\} \quad (46)$$

Then the primal and dual base models can be written:

$$\boxed{\begin{array}{ll} \text{Find } (e_0, \varepsilon_0) \in V \times V \text{ such that} \\ \quad B(u_0; v) + B'(u_0; e_0, v) + \Delta_4(u_0, e_0, v) = F(v), & \forall v \in V \\ \quad B'(u_0; v, p_0) + B'(u_0; v, \varepsilon_0) + \Delta_6(u_0, v, e_0, p_0 + \varepsilon_0) \\ \qquad\qquad\qquad = Q'(u_0; v) + \Delta_5(u_0, e_0, v), & \forall v \in V \end{array}} \quad (47)$$

Thus, the errors e_0 and ε_0 satisfy the following equations:

$$B'(u_0; e_0, v) + \Delta_4(u_0, e_0, v) = \mathcal{R}(u_0; v), \qquad \forall v \in V$$
$$B'(u_0; v, \varepsilon_0) + \Delta_6(u_0, v, e_0, p_0 + \varepsilon_0) \qquad\qquad\qquad (48)$$
$$\qquad\qquad = \bar{\mathcal{R}}(u_0, p_0; v) + \Delta_5(u_0, e_0, v), \qquad \forall v \in V$$

where $\mathcal{R}(u_0; v)$ and $\bar{\mathcal{R}}(u_0, p_0; v)$ are the residual functionals in (12) and (16).

If $B(\cdot;\cdot)$ and $Q(\cdot)$ are a bilinear form and a linear form, respectively, then Δ_4, Δ_5, and Δ_6 vanish, $B' = B$, $Q' = Q$, so that the errors are governed by:

$$B(e_0, v) = \mathcal{R}(u_0; v), \qquad \forall v \in V$$
$$B(v, \varepsilon_0) = \bar{\mathcal{R}}(u_0, p_0; v), \qquad \forall v \in V$$

22

Otherwise, we shall assume that constants $C_4 = C_4(u_0)$, $C_5 = C_5(u_0)$, and $C_6 = C_6(u_0, p_0)$ exist such that:

$$\left.\begin{array}{l} |\Delta_4(u_0, e_0, v)| \le C_4 \|e_0\|^2 \|v\| \\[4pt] |\Delta_5(u_0, e_0, v)| \le C_5 \|e_0\| \, \|v\| \\[4pt] |\Delta_6(u_0, v, e_0, p_0 + \varepsilon_0)| \le C_6 \|e_0\| \, \|v\| \end{array}\right\} \tag{49}$$

and that it is possible to find a $u_0 \in V$ such that $\infty > \alpha(u_0), \beta(u_0) > 0$, where $\alpha(u_0)$ and $\beta(u_0)$ are given by

$$\alpha(u_0) = \inf_{w \in V \setminus \{0\}} \sup_{v \in V \setminus \{0\}} \frac{|B'(u_0; w, v)|}{\|w\| \, \|v\|} \ge 0$$

$$\beta(u_0) = \inf_{w \in V \setminus \{0\}} \sup_{v \in V \setminus \{0\}} \frac{|B'(u_0; v, w)|}{\|w\| \, \|v\|} \ge 0$$

Then we easily obtain:

$$\alpha(u_0)\|e_0\| \le \|\mathcal{R}(u_0)\|_* + C_4 \|e_0\|^2$$

$$\beta(u_0)\|\varepsilon_0\| \le \|\bar{\mathcal{R}}(u_0, p_0)\|_* + (C_5 + C_6)\|e_0\|$$

where $\| \cdot \|_*$ denotes the norm on the dual space V':

$$\|\mathcal{R}(u_0)\|_* = \sup_{v \in V \setminus \{0\}} \frac{|\mathcal{R}(u_0; v)|}{\|v\|}$$

$$\|\bar{\mathcal{R}}(u_0, p_0)\|_* = \sup_{v \in V \setminus \{0\}} \frac{|\bar{\mathcal{R}}(u_0, p_0; v)|}{\|v\|}$$

These results show that for e_0 sufficiently small, when the assumed properties prevail, the modeling errors e_0 and ε_0 are globally bounded by the norms of the residuals.

7 Examples

7.1 Nano-indentation application

In this section, we consider the problem of determining static equilibrium configurations of a regular lattice of N atoms. The base problem is derived by minimization of the potential energy of the system involving all atoms in the lattice. However, for many applications, the base problem is intractable due to the very large number of atoms N. In order to decrease the complexity of the base problem, the quasicontinuum method [53, 54, 55] is a popular approach for constructing surrogate problems which aim at reducing the number of active atoms in the lattice needed in computer simulations.

7.1.1 The base problem

Let $\mathcal{L}$ be a regular lattice of N atoms in $\mathbb{R}^d$, $d = 2$ or 3. The positions of the atoms in the reference configuration are given by the vectors $\hat{\boldsymbol{x}}_i \in \mathbb{R}^d$, $i = 1, \ldots, N$ and in the
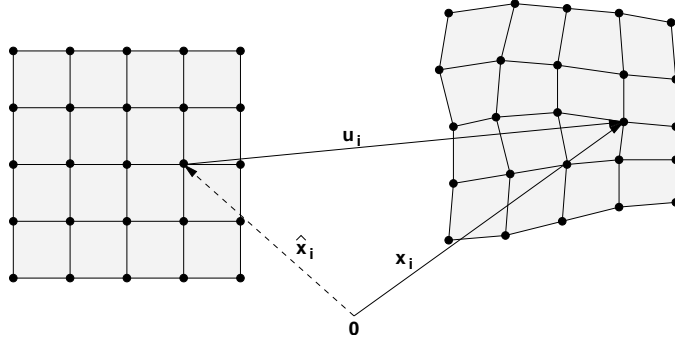
Figure 3: Reference configuration and deformed configuration of a model lattice.

equilibrium configuration by $\boldsymbol{x}_i = \hat{\boldsymbol{x}}_i + \boldsymbol{u}_i$, $i = 1, \ldots, N$, where $\boldsymbol{u}_i$ is the displacement of atom i (see Fig. 3). We assume that the lattice in the reference configuration covers the region $\bar{\Omega}$, where Ω is an open bounded set of $\mathbb{R}^d$ with boundary $\partial\Omega$. For a more detailed analysis, see [42]. We introduce the finite-dimensional vector space $V = (\mathbb{R}^d)^N$, and we use the notation $\boldsymbol{u} = (\boldsymbol{u}_1, \boldsymbol{u}_2, \ldots, \boldsymbol{u}_N) \in V$, to refer to the displacements of the collection of N atoms. The total potential energy of the system is assumed to be the sums:

$$E(\boldsymbol{u}) = -\sum_{i=1}^{N} \boldsymbol{f}_i \cdot \boldsymbol{u}_i + \sum_{k=1}^{N} E_k(\boldsymbol{u}) \tag{50}$$

where $\boldsymbol{f}_i$ is the external load applied to an interior atom i and $E_k(\boldsymbol{u})$ is the energy of atom k determined from inter-atomic potentials.

The goal of molecular statics is to find the equilibrium state $\boldsymbol{u} \in V$ that minimizes the total potential energy of the system, i.e. $E(\boldsymbol{u}) = \inf_{\boldsymbol{v} \in V} E(\boldsymbol{v})$. This minimization problem can be recast into the variational problem:

$$Find\ \boldsymbol{u} \in V\ \ such\ that\quad B(\boldsymbol{u}; \boldsymbol{v}) = F(\boldsymbol{v}), \quad \forall \boldsymbol{v} \in V \tag{51}$$

where, for any $\boldsymbol{u} \in V$ and $\boldsymbol{v} \in V$,

$$B(\boldsymbol{u}; \boldsymbol{v}) = \sum_{i=1}^{N} \left[\sum_{k=1}^{N} \frac{\partial E_k}{\partial \boldsymbol{u}_i}(\boldsymbol{u}) \right] \cdot \boldsymbol{v}_i$$
$$F(\boldsymbol{v}) = \sum_{i=1}^{N} \boldsymbol{f}_i \cdot \boldsymbol{v}_i \tag{52}$$

Here $\partial/\partial\boldsymbol{u}_i$ is the gradient vector with respect to each component $u_{\alpha,i}$ of the displacement vector $\boldsymbol{u}_i$, i.e. $\partial/\partial\boldsymbol{u}_i = (\partial/\partial u_{1,i}, \ldots, \partial/\partial u_{d,i})$.

7.1.2 The surrogate problem by the quasicontinuum method

We briefly recall the main features of the quasicontinuum method (QCM). For more details, see [53, 49, 28]. The objectives of the method are essentially twofold:

1. dramatically reduce the number of degrees of freedom from $N \times d$.

2. substantially lower the cost in the calculation of the potential energy by computing energies only at selected sites.

The approach becomes very efficient if one considers an adaptive scheme to automatically select the degrees of freedom that allow one to capture the critical deformations of the lattice.

The first step consists of choosing a set of R representative atoms, the so-called "repatoms", and of approximating $\boldsymbol{u} \in V$ by a reduced vector $\boldsymbol{u}_0 \in W = (\mathbb{R}^d)^R$, $R \ll N$, with $\boldsymbol{u}_0 = (\boldsymbol{u}_{0,1}, \boldsymbol{u}_{0,2}, \ldots, \boldsymbol{u}_{0,R}) \in W$. The displacements $\boldsymbol{u}_0$ represent the active degrees of freedom of the system and the repatoms are conveniently identified with the nodes of a finite element partition $\mathcal{P}_h$ of Ω. The displacements of the $(N - R)$ slave atoms are then interpolated from $\boldsymbol{u}_0$ by piecewise linear polynomials using the finite element mesh. Indeed, let ϕ_r, $r = 1, \ldots, R$, be the basis functions (the hat functions) associated with the mesh $\mathcal{P}_h$. We can construct a finite element vector function $\boldsymbol{u}_h$ such that

$$\boldsymbol{u}_h(\boldsymbol{x}) = \sum_{r=1}^{R} \boldsymbol{u}_{0,r} \phi_r(\boldsymbol{x}), \qquad \forall \boldsymbol{x} \in \bar{\Omega}. \tag{53}$$

The displacements of the N atoms in the lattice are obtained via the extension operator $\Pi : W \to V$ defined such that

$$(\Pi \boldsymbol{u}_0)_i = \boldsymbol{u}_h(\boldsymbol{x}_i), \qquad i = 1, \ldots, N. \tag{54}$$

The second step of the QCM is devoted to the approximation of the total energy $E(\Pi \boldsymbol{u}_0)$ by summing only over the repatoms such that:

$$E(\Pi \boldsymbol{u}_0) \approx E_0(\boldsymbol{u}_0) = -\sum_{r=1}^{R} n_r \, \boldsymbol{f}_{0,r} \cdot \boldsymbol{u}_{0,r} + \sum_{r=1}^{R} n_r E_r(\boldsymbol{u}_0) \tag{55}$$

where n_r is an appropriate weight function associated with repatom r so as to account for all atoms in the lattice, i.e. $\sum_r n_r = N$, and $\boldsymbol{f}_{0,r}$ is the averaged external force acting on repatom r. The interatomic energies $n_r E_r(\boldsymbol{u}_0)$ are further approximated by considering a repatom to be either "local" or "nonlocal". The term "local" refers to the fact that the energy at a point in the continuum depends on the deformation at that point only and not on its surroundings. Let R_{lc} denote the number of local repatoms and R_{nl} the number of nonlocal repatoms, $R = R_{lc} + R_{nl}$. The atomistic energies are now separated into local and nonlocal contributions such as:

$$\sum_{r=1}^{R} n_r E_r(\boldsymbol{u}_0) = \sum_{r=1}^{R_{lc}} n_r E_r^{loc}(\boldsymbol{u}_0) + \sum_{s=1}^{R_{nl}} n_s E_s^{nl}(\boldsymbol{u}_0) \tag{56}$$

Note that for $R_{nl} = 0$, the method is called the *local QCM*, for $R_{lc} = 0$, the *nonlocal QCM*. Otherwise, the method is referred to as the *coupled local/nonlocal QCM*. We shall only consider the latter in what follows. For a detailed description on how

these energies are calculated, see [28]. The approximation of the energy by the coupled local/nonlocal approach yields non-physical forces, the so-called ghost forces, at the interface of the local and nonlocal regions. In the QCM, corrective forces are added to balance these ghost forces (see e.g. [49]). We also observe that the local QCM is comparable to a homogenization process in which the energies of the slave atoms are approximated based on the Cauchy-Born hypothesis, which postulates that when a monatomic crystal is subjected to a small linear boundary displacement, all atoms within the crystal follow this linear displacement pattern. Stated in another way, when the boundaries of a representative volume of atoms in a lattice are subjected to a linear displacement field, the volume experiences a homogeneous deformation. Friesecke and Theil [20] have demonstrated that this hypothesis can fail in the case of the so-called "unfavourable" lattice parameters, but that in many cases it can be rigorously proved to hold.

Remark 6 *The local/nonlocal criterion: The selection of representative atoms as local or nonlocal is based upon the variation of the deformation gradient on the atomic scale in the vicinity of the atoms. A repatom is made local if the deformation is almost uniform, nonlocal if the deformation gradient is large. In the QCM, the deformation gradients are compared elementwise by computing the differences between the eigenvalues of the right stretch tensor $\boldsymbol{U}^2 = \boldsymbol{F}^T\boldsymbol{F}$ in each element, $\boldsymbol{F}$ being the deformation gradient in the element.* $\square$

The minimization of the energy $E_0(\boldsymbol{u}_0)$ yields the surrogate problem:

$$Find \ \boldsymbol{u}_0 \in W \ such \ that \quad B_0(\boldsymbol{u}_0; \boldsymbol{v}) = F_0(\boldsymbol{v}), \quad \forall \boldsymbol{v} \in W \tag{57}$$

where the semilinear form $B_0(\cdot; \cdot)$ and linear form $F_0(\cdot)$ are defined as

$$
\begin{aligned}
B_0(\boldsymbol{u}; \boldsymbol{v}) &= \sum_{i=1}^{R} \left[\sum_{r=1}^{R} n_r \frac{\partial E_r}{\partial \boldsymbol{u}_i}(\boldsymbol{u}) \right] \cdot \boldsymbol{v}_i \\
F_0(\boldsymbol{v}) &= \sum_{i=1}^{R} n_i \, \boldsymbol{f}_{0,i} \cdot \boldsymbol{v}_i
\end{aligned}
\tag{58}
$$

Remark 7 *In [53, 49, 28] it is proposed that an automatic mesh adaption technique be used to add and remove representative atoms "on the fly", in order to capture the fine features during the simulation. The criterion for adaptivity is based upon the derivation of an error indicator similar to that of Zienkiewicz and Zhu [62] for the finite element method. This adaptive strategy will be used as is to compute the solution $\boldsymbol{u}_0$ and an overkill solution of the problem. Our goal here is to propose an alternative scheme which will allow one to adapt the mesh by controlling error in a quantity of interest.* $\square$

7.1.3 Error estimation and adaptivity

The errors in the solution $\boldsymbol{u}_0$ obtained by the QCM, with respect to the solution of the base problem, arise from three sources: 1) the nonlinear problem is solved

approximately by an iterative method, 2) the reduction of the number of degrees of freedom from N to R, 3) the approximation of the total potential energy by E_0, as defined in (55) and (56).

The error due to the nonlinear solver is controlled at each iteration and is assumed to be negligible compared to the other sources of error. This error is sometimes referred to as the *solution error*. The second type of error is analogous to *discretization error* in Galerkin approximations such as in the finite element method. Here it can be regarded as a model reduction error. Finally, the last source induces a so-called *modeling error* due to the modeling of the energy using the coupled local/nonlocal QCM. In this work, we will not differentiate between the three types of errors and will provide for estimates of the total error.

In the nanoindentation problem that will be presented in the next section, the quantity of interest is the force that the crystal exerts on the indenter. Let the atoms, in contact with the lower surface of the indenter, be numbered from 1 to M. The quantity of interest is

$$Q(\boldsymbol{u}) = -\sum_{i=1}^{M} f_{y,i} = -\sum_{i=1}^{M} \frac{\partial E_i}{\partial u_{y,i}}(\boldsymbol{u}) \tag{59}$$

where $f_{y,i}$ and $u_{y,i}$ are the force and the displacement in the y-direction with respect to atom i. We assume that the meshes are such that the M atoms under the indenter are representative atoms, and all the forces are computed by the nonlocal approach. The objective is then to estimate the error quantity

$$\mathcal{E} = Q(\boldsymbol{u}) - Q(\Pi\boldsymbol{u}_0). \tag{60}$$

The dual problem associated with the base problem (51) reads:

$$\text{Find } \boldsymbol{p} \in V \text{ such that } \quad B'(\boldsymbol{u}; \boldsymbol{v}, \boldsymbol{p}) = Q'(\boldsymbol{u}; \boldsymbol{v}), \quad \forall \boldsymbol{v} \in V \tag{61}$$

where the derivatives are given in the molecular statics case by

$$B'(\boldsymbol{u}; \boldsymbol{v}, \boldsymbol{p}) = \sum_{j=1}^{N} \sum_{i=1}^{N} \boldsymbol{v}_j \cdot \left[\sum_{k=1}^{N} \frac{\partial^2 E_k}{\partial \boldsymbol{u}_j \partial \boldsymbol{u}_i}(\boldsymbol{u}) \right] \cdot \boldsymbol{p}_i$$
$$Q'(\boldsymbol{u}; \boldsymbol{v}) = -\sum_{j=1}^{N} \boldsymbol{v}_j \cdot \left[\sum_{i=1}^{M} \frac{\partial^2 E_i}{\partial \boldsymbol{u}_j \partial u_{y,i}}(\boldsymbol{u}) \right] \tag{62}$$

The surrogate dual problem is then,

$$\text{Find } \boldsymbol{p}_0 \in W \text{ such that } \quad B_0'(\boldsymbol{u}_0; \boldsymbol{v}, \boldsymbol{p}_0) = Q_0'(\boldsymbol{u}_0; \boldsymbol{v}), \quad \forall \boldsymbol{v} \in W \tag{63}$$

where by Q_0 we mean $Q_0(\boldsymbol{v}) = Q(\Pi\boldsymbol{v})$. The errors $\boldsymbol{e}_0 \in V$ and $\boldsymbol{\varepsilon}_0 \in V$ in $\Pi\boldsymbol{u}_0$ and $\Pi\boldsymbol{p}_0$, respectively, are defined as $\boldsymbol{e}_0 = \boldsymbol{u} - \Pi\boldsymbol{u}_0$ and $\boldsymbol{\varepsilon}_0 = \boldsymbol{p} - \Pi\boldsymbol{p}_0$. Then, the error in $Q(\boldsymbol{u})$ produced by $\Pi\boldsymbol{u}_0$ is given by, using Theorem 1,

$$\mathcal{E} = Q(\boldsymbol{u}) - Q(\Pi\boldsymbol{u}_0) = \mathcal{R}(\Pi\boldsymbol{u}_0; \boldsymbol{p}) + \Delta_1(\Pi\boldsymbol{u}_0, \Pi\boldsymbol{p}_0, \boldsymbol{e}_0, \boldsymbol{\varepsilon}_0) \tag{64}$$

where $\mathcal{R}(\Pi \boldsymbol{u}_0; \boldsymbol{v})$ is the residual functional, with respect to the base model problem

$$\mathcal{R}(\Pi \boldsymbol{u}_0; \boldsymbol{v}) = F(\boldsymbol{v}) - B(\Pi \boldsymbol{u}_0; \boldsymbol{v}), \quad \boldsymbol{v} \in V. \tag{65}$$

We now propose an approach to estimate the quantity $\mathcal{R}(\Pi \boldsymbol{u}_0; \boldsymbol{p})$. On one hand, we may simply consider computing $\mathcal{R}(\Pi \boldsymbol{u}_0; \Pi \boldsymbol{p}_0)$. But this term would fail to pick up the model reduction error as in Galerkin methods. In other words, a better approximation of the dual solution should be sought in a space larger than W. Our second observation is concerned with the evaluation of the residual

$$\begin{aligned}
\mathcal{R}(\Pi \boldsymbol{u}_0; \boldsymbol{p}) &= F(\Pi \boldsymbol{u}_0, \boldsymbol{p}) - B(\Pi \boldsymbol{u}_0; \boldsymbol{p}) \\
&= \sum_{i=1}^{N} \left(\boldsymbol{f}_i - \left[\sum_{k=1}^{N} \frac{\partial E_k}{\partial \boldsymbol{u}_i}(\Pi \boldsymbol{u}_0) \right] \right) \cdot \boldsymbol{p}_i = \sum_{i=1}^{N} \boldsymbol{r}_i(\Pi \boldsymbol{u}_0) \cdot \boldsymbol{p}_i
\end{aligned} \tag{66}$$

where the residual vector $\boldsymbol{r}(\Pi \boldsymbol{u}_0) \in V$ indicates how the forces acting on each atom i fail to be equilibrated. It is well known that calculation of atomic forces is cost-prohibitive when N is large. In an effort to reduce the computational cost of the error estimator, it is desired to take into account only the most significant contributions to $\boldsymbol{r}(\Pi \boldsymbol{u}_0)$. Towards this goal, we propose to evaluate the residual and the dual solution on a mesh which is finer than the mesh used for the evaluation of $\boldsymbol{u}_0$, but coarser than the mesh involving all atoms as nodes.

Let $\tilde{\mathcal{P}}_h$ denote such a partition of $\bar{\Omega}$ with $\tilde{N}$ nodes, $R < \tilde{N} \ll N$. In practice, the mesh $\tilde{\mathcal{P}}_h$ is constructed using the adaptive technique described in Remark 7. We introduce the vector space $\tilde{V} = (\mathbb{R}^d)^{\tilde{N}}$, the extension operator $\tilde{\Pi} : W \to \tilde{V}$, and the residual functional $\tilde{\mathcal{R}}$ on $\tilde{V}$,

$$\tilde{\mathcal{R}}(\tilde{\boldsymbol{u}}; \tilde{\boldsymbol{v}}) = \sum_{i=1}^{\tilde{N}} \tilde{\boldsymbol{r}}_i(\tilde{\boldsymbol{u}}) \cdot \tilde{\boldsymbol{v}}_i \tag{67}$$

where $\tilde{\boldsymbol{u}}, \tilde{\boldsymbol{v}} \in \tilde{V}$, and the $\tilde{\boldsymbol{r}}_i(\tilde{\boldsymbol{u}})$ are computed via the coupled local/nonlocal QCM. We also consider the new dual problem on $\tilde{V}$:

$$Find \ \tilde{\boldsymbol{p}} \in \tilde{V} \ such \ that \quad \tilde{B}'(\tilde{\Pi} \boldsymbol{u}_0; \tilde{\boldsymbol{v}}, \tilde{\boldsymbol{p}}) = \tilde{Q}'(\tilde{\Pi} \boldsymbol{u}_0; \tilde{\boldsymbol{v}}), \quad \forall \tilde{\boldsymbol{v}} \in \tilde{V} \tag{68}$$

with

$$\begin{aligned}
\tilde{B}(\tilde{\boldsymbol{u}}; \tilde{\boldsymbol{v}}) &= \sum_{i=1}^{\tilde{N}} \left[\sum_{k=1}^{\tilde{N}} n_k \frac{\partial E_k}{\partial \boldsymbol{u}_i}(\tilde{\boldsymbol{u}}) \right] \cdot \tilde{\boldsymbol{v}}_i \\
\tilde{Q}(\tilde{\boldsymbol{u}}) &= - \sum_{i=1}^{M} \frac{\partial E_i}{\partial u_{y,i}}(\tilde{\boldsymbol{u}})
\end{aligned} \tag{69}$$

The error estimator with respect to the quantity of interest Q is defined as the computable quantity

$$\eta = \tilde{\mathcal{R}}(\tilde{\Pi} \boldsymbol{u}_0; \tilde{\boldsymbol{p}}) = \sum_{i=1}^{\tilde{N}} \tilde{\boldsymbol{r}}_i(\tilde{\Pi} \boldsymbol{u}_0) \cdot \tilde{\boldsymbol{p}}_i \tag{70}$$

and we will show in the next subsection that η is a reasonable estimate of the error $\mathcal{E} = Q(\boldsymbol{u}) - Q_0(\boldsymbol{u}_0) = Q(\boldsymbol{u}) - Q(\Pi\boldsymbol{u}_0)$. The quality of the estimates will be measured as usual in terms of the effectivity index λ, defined as the ratio of the estimated error to the actual error, assuming the latter is known,

$$\lambda = \frac{\eta}{Q(\boldsymbol{u}) - Q_0(\boldsymbol{u}_0)} \tag{71}$$

For adaptation purposes, the quantity η is decomposed into elementwise contributions η_K such that:

$$\eta = \sum_{K=1}^{N_e} \eta_K \tag{72}$$

This is accomplished in practice as follows: for any element K, we have the nodal value $\eta_i^K = \tilde{\boldsymbol{r}}_i(\tilde{\Pi}\boldsymbol{u}_0) \cdot \tilde{\boldsymbol{p}}_i$. We then compute the integral average of the linear interpolant over the element, namely

$$\eta_K(\boldsymbol{x}) = \left| \frac{1}{|K|} \int_K \sum_{i=1}^3 \eta_i^K \phi_i(\boldsymbol{x}) \, dx \right|, \qquad \boldsymbol{x} \in K \tag{73}$$

where $|K|$ is the area of the element K and $\phi_i(\boldsymbol{x})$ are the linear hat functions described in (53). The adaptivity algorithm then proceeds as follows:

1. Initialize the load step s $= 0$. Input user-tolerance δ_{tol}.

2. s $=$ s+1.

3. Solve the primal and dual problems.

4. Compute the error estimate.

5. Check: $|\eta| > \delta_{\text{tol}}|Q(\boldsymbol{u}_0)|$. If false: go to Step 2. If true: mark those elements with $|\eta_K(\tilde{\Pi}\boldsymbol{u}_0, \tilde{\boldsymbol{p}})| > \alpha \max_K |\eta_K(\tilde{\Pi}\boldsymbol{u}_0, \tilde{\boldsymbol{p}})|$, where α is a user-supplied number between 0 and 1.

6. Refine flagged elements and go to Step 3.

7.1.4   A numerical example

The performance of the error estimator and adaptive strategy is demonstrated for a nano-indentation problem proposed by Tadmor *et al.* [41, 49, 54]. The simulation is actually provided as a model example accompanying the open source software package [29]. In this example, a thin film of aluminum crystal is indented by a rigid rectangular indenter, 9.31 Å wide and infinite in the out-of-plane direction, as depicted in Fig. 4. The dimensions for the block of crystal are 2000×1000 (in Angströms) in the [111] and [$\bar{1}$10] directions of the crystal. The crystal rests on a rigid support so that homogeneous boundary conditions $\boldsymbol{u}_i = \boldsymbol{0}$ are prescribed for those atoms i located at $y = 0$. The indenter is moved downward in a succession of 30 load-step increments $\delta l = 0.2$. The boundary conditions for the atoms i just below the indenter are given
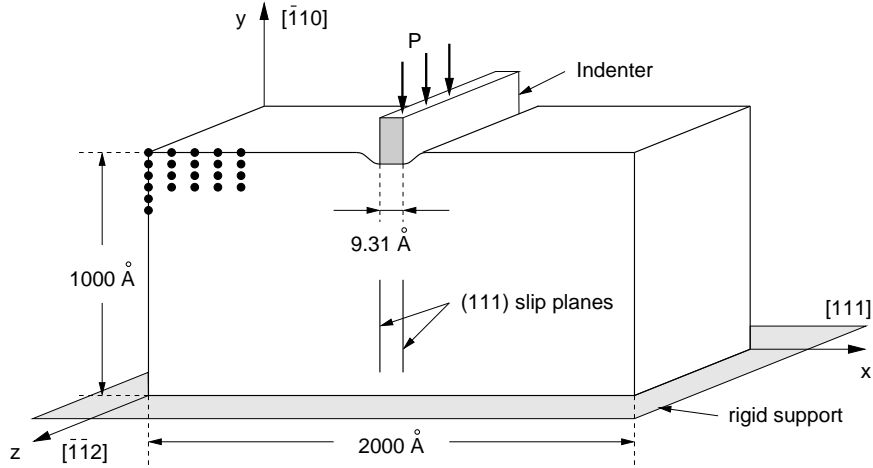
Figure 4: Nano-indentation of an aluminum crystal (the schematic representation is inspired from Fig. 1 in [54]).

by: $\boldsymbol{u}_i = (0, -m\,\delta l, 0)$, $m = 1, \ldots, 30$. Quasistatic steps are then considered to solve for the displacements.

The site energies $E_k(\boldsymbol{u})$ of each atom k of the aluminum crystal are computed here using the Embedded Atom Method (EAM) atomistic model (see e.g. [12, 18]). Briefly, the semi-empirical potential energy for atom k is given by the sum of of an electron-density dependent embedding energy and pairwise interatomic potentials. Note that the QCM employs a cutoff function to approximate the interatomic potentials as the potential function decays rapidly with respect to the interatomic distance.

The interatomic distances in the undeformed configuration of the crystal are 2 Å and 2 Å in the x- and y-direction, respectively. One $(\bar{1}, \bar{1}, 0)$ layer of the film contains about $500{,}000$ atoms. In this example, we perform a pseudo-two-dimensional analysis of the QCM in the sense that the displacement vectors are constrained to be independent of the z-variable. However, all atomistic energies are computed in three dimensions [54]. Rather than solving for the solution $\boldsymbol{u}$ of the full base problem (51), we have opted to consider as our reference solution an "overkill" solution of the surrogate problem (57). This solution is hereafter referred to as the base model solution as it involves a sufficiently high number of degrees of freedom so that it is a very accurate approximation of $\boldsymbol{u}$.

The base model solution is compared to the solution $\boldsymbol{u}_0$ obtained by the quasicontin-uum method on a much coarser discretization (see Fig. 5). The vertical displacements of the base model and the QC solution are compared in Fig. 6 while the y-component of the dual solutions are shown in Fig. 7. In the QC solution, the refinement parameter was set according to the authors recommendations [29] to .075 while the Goals solution was set to a 5 percent error tolerance in the quantity of interest. Notice in Fig. 6 how the base model solution allows the slip plane to propagate into the material much more quickly than the QC solution. Furthermore, notice in Fig. 7 how the dual solution for the base model displays the influence of the slip plane on the quantity of interest as the dislocations nucleate and move. In contrast, the mesh produced by the QCM lacks

the resolution to capture this effect.

Next, the force under the indenter is shown in Fig. 8 for the base model solution, the QC solution, and the Goals algorithm. This force represents a quantity of physical interest as it can be experimentally measured and clearly indicates the nucleation of the dislocation. Note that the base model has been run only until load step 27 due to the limitation in the computational resources. The other two solutions have been completed and are fully displayed. The QCM produces a stiffer material so that the critical force for dislocation nucleation occurs one load step earlier than the base model solution. On the other hand, the Goals solution produces a remarkably accurate representation of the force-displacement curve when compared to the base model. Shown in Fig. 9 are the relative errors and effectivity indices for each load step, demonstrating the effectiveness of the error estimator used. Note the effectivity index at loadstep 2 is far from unity due to the fact that the error is near zero while the estimate is far from it. As can be seen, the error in the solution is controlled to within the preset tolerance of 5 percent with the exception of the third and final load steps. Although the error estimator overestimates the exact error for most of the loadsteps in this example, this behavior may not be true for other cases. It is not proved that this is a guaranteed upper bound. The solution during load step 2 exhibits a behavior that we have not been able to understand at this point. This will be the subject of future analysis.

Finally, Figs. 10, 11, and 12 compare the mesh, the primal, and the dual solutions between the QCM and Goals methods for load step 27 (after the dislocation has nucleated and the force drop observed). Notice in Fig. 10 that the Goals solution has refined many atoms near the indenter and the surrounding region of the slip plane. While the primal solutions in Fig. 11 look similar, the dual solutions in 12 are somewhat different. This is a reflection of the fact that primal solution has not converged in the QCM case thereby corrupting the accuracy of the dual solution.

7.2 Molecular dynamics application

We present in this section an application to modeling the dynamics of atoms whose motion is determined by molecular dynamics principles. We consider here surrogate models generated by the bridging scale method (BSM) of Wagner and Liu [60] and the pseudo-spectral multiscale method (PMM) of Tang *et al.* [57]. We will show only preliminary results, but future work will include the development of automatic model adaptivity algorithms and the investigation of other surrogate models such as that put forth by Xiao and Belytschko [61].

7.2.1 The base model

Let $\Omega \subset \mathbb{Z}^d$ be an open bounded set, $d = 1$, 2, or 3. Let $\mathcal{L}$ denote the lattice of n atoms covering $\overline{\Omega}$. The initial positions of the atoms are given by the vectors $\boldsymbol{x}_i \in \mathbb{R}^d$ and the respective displacements by $\boldsymbol{u}_i \in \mathbb{R}^d$, $i = 1, \ldots, n$. The notation $\boldsymbol{u} = (\boldsymbol{u}_1, \boldsymbol{u}_2, \ldots, \boldsymbol{u}_n)$ collectively represents the displacement of the n atoms. We denote by $\boldsymbol{M}$ the mass matrix of the system, $M_{ij} = m_{(i)} \delta_{ij}$, where m_i is the mass of atom i. Additionally, the interatomic potential energy (assumed to be given) is represented by $E(\boldsymbol{u})$ and the interatomic forces are computed as $\boldsymbol{f}(\boldsymbol{u}) = -\partial_{\boldsymbol{u}} E(\boldsymbol{u})$.
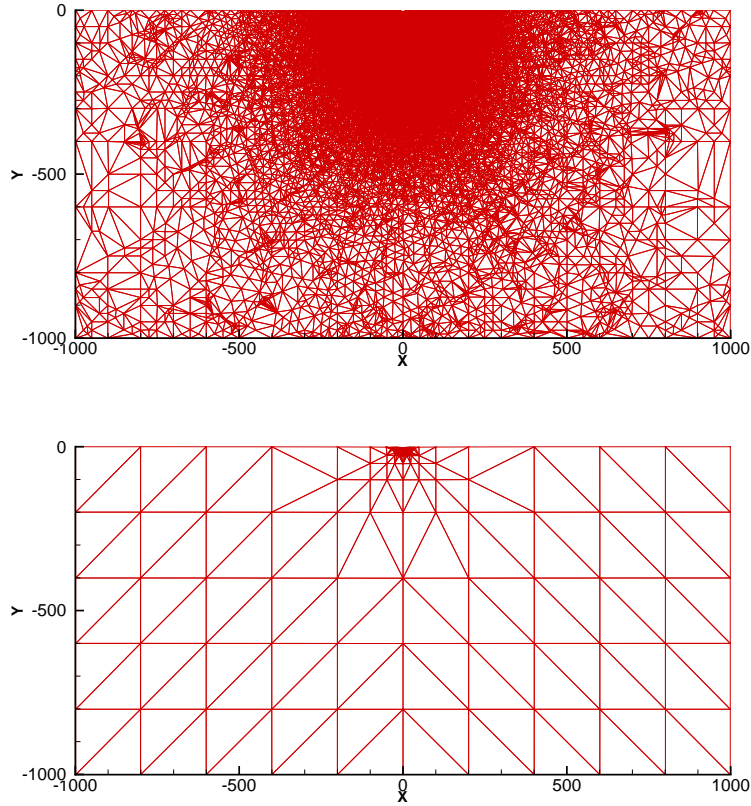
Figure 5: Finite element triangulation for the base model solution (above) and the QC solution (below). The base model mesh is shown at load step 26 while the QC solution is shown at load step 25 (just prior to dislocation nucleation in both cases). The base model has 40554 atoms while the QC solution has 492 active atoms.
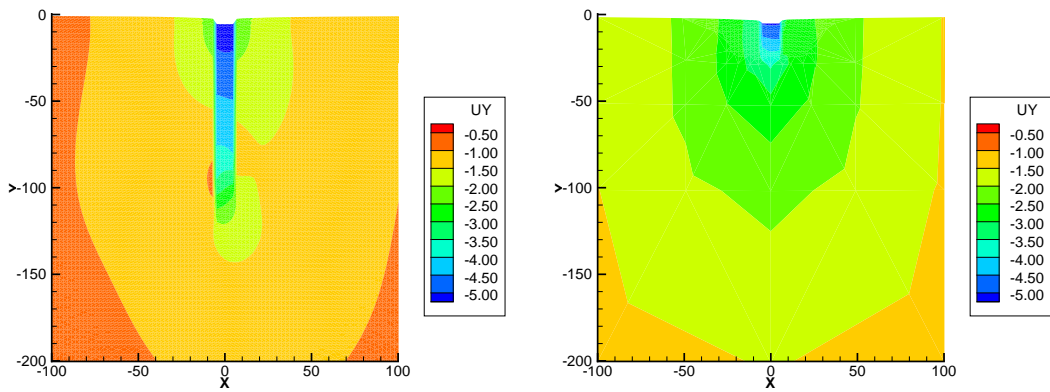

Figure 6: Base model (left) and QC (right) primal solutions at the beginning of dislocation nucleation.
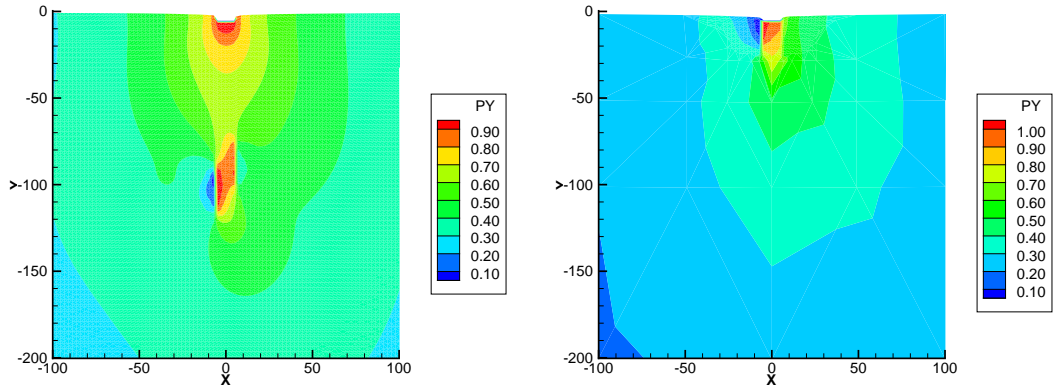
Figure 7: Base model (left) and QC (right) dual solutions at the beginning of dislocation nucleation.
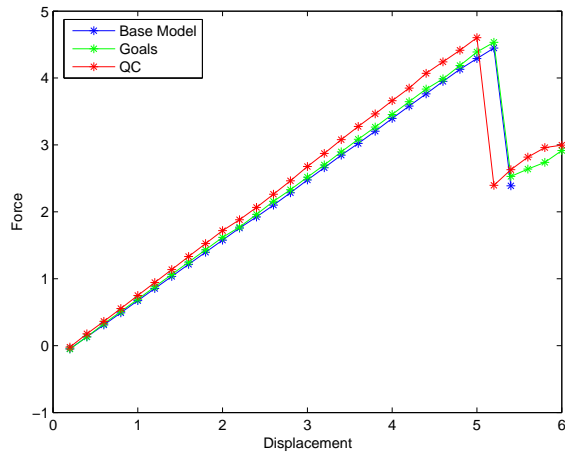

Figure 8: Force-displacement curve comparing the evolution of the base model, QC, and Goals solutions.
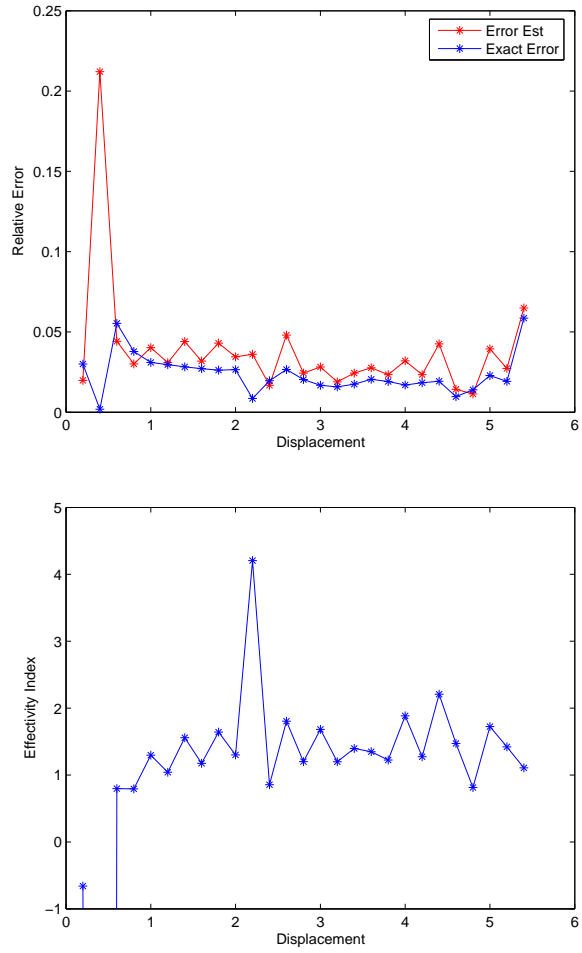
33

Figure 9: Exact and estimated relative errors for the Goals solution (top). Effectivity indices (bottom).
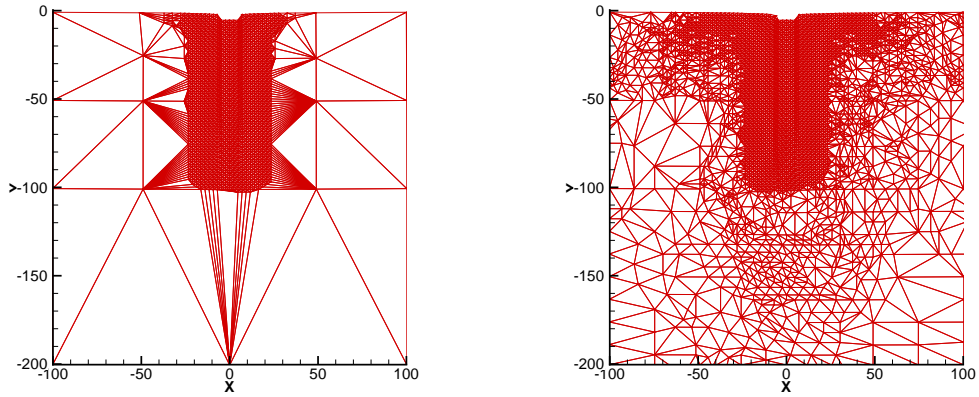
Figure 10: QC (left) and Goals (right) meshes at load step 27. The numbers of atoms in the QC mesh and the Goals mesh are 1629 and 3452.
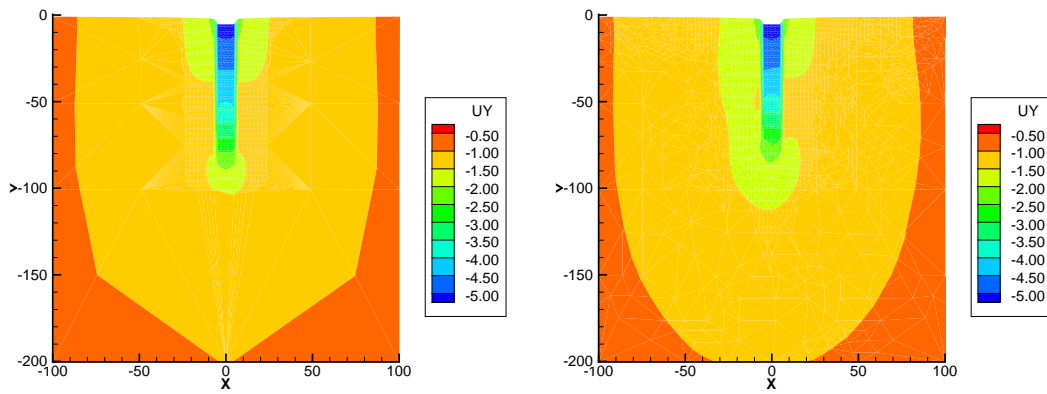

Figure 11: Comparison of the primal solution of the QCM algorithm (left) and the Goals algorithm (right) at load step 27.
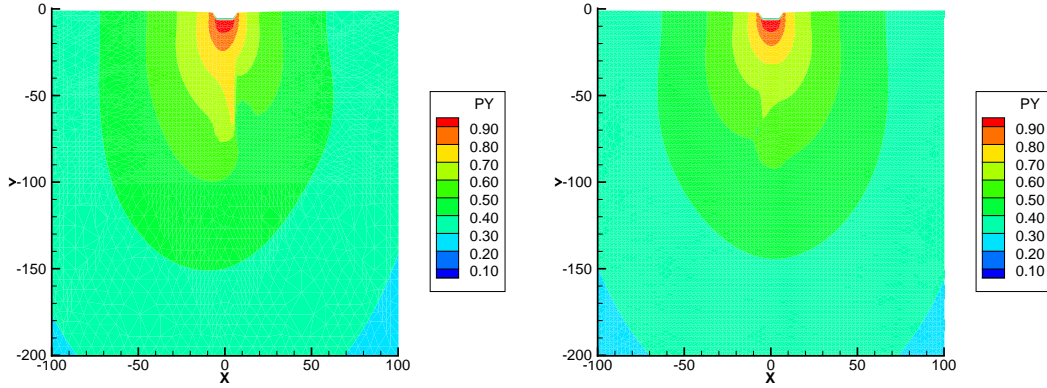
Figure 12: Comparison of the dual solution of the QCM algorithm (left) and the Goals algorithm (right) at load step 27.

The molecular dynamics (MD) problem is then characterized by the following system of ordinary differential equations for the displacements $\boldsymbol{u} = \boldsymbol{u}(t)$:

$$\boldsymbol{M}\ddot{\boldsymbol{u}} = \boldsymbol{f}(\boldsymbol{u}), \quad \boldsymbol{u}(0) = \boldsymbol{U}_0, \quad \dot{\boldsymbol{u}}(0) = \boldsymbol{V}_0 \tag{74}$$

subjected to appropriate boundary conditions. Note that external forces on the atoms have been neglected for simplicity. The superimposed dot implies differentiation with respect to time. Assuming $\boldsymbol{u}, \boldsymbol{v} \in \mathbb{V} = C^2\left((0,T); \left(\mathbb{R}^d\right)^n\right)$, we may recast the above problem into the weak form (1) with:

$$B(\boldsymbol{u}; \boldsymbol{v}) = \int_0^T \boldsymbol{v}^T\left(\boldsymbol{M}\ddot{\boldsymbol{u}} - \boldsymbol{f}(\boldsymbol{u})\right) dt + \boldsymbol{v}^T(0)\boldsymbol{M}\dot{\boldsymbol{u}}(0) - \dot{\boldsymbol{v}}^T(0)\boldsymbol{M}\boldsymbol{u}(0)$$
$$F(\boldsymbol{v}) = \boldsymbol{v}^T(0)\boldsymbol{M}\boldsymbol{V}_0 - \dot{\boldsymbol{v}}^T(0)\boldsymbol{M}\boldsymbol{U}_0 \tag{75}$$

Note that the initial conditions in the above formulation are weakly imposed. Similarly, it is not difficult to derive the first derivative of the semilinear form $B(\cdot; \cdot)$. Indeed, we have for $\boldsymbol{p}, \boldsymbol{v} \in \mathbb{V}$,

$$B'(\boldsymbol{u}; \boldsymbol{v}, \boldsymbol{p}) = \int_0^T \left(\boldsymbol{M}\ddot{\boldsymbol{p}} - (\boldsymbol{f}'(\boldsymbol{u}))^T\boldsymbol{p}\right)^T \boldsymbol{v} \, dt$$
$$+ (\boldsymbol{M}\boldsymbol{p}(T))^T\dot{\boldsymbol{v}}(T) - (\boldsymbol{M}\dot{\boldsymbol{p}}(T))^T\boldsymbol{v}(T) \tag{76}$$

where $\boldsymbol{f}'(\boldsymbol{u}) = \partial_{\boldsymbol{u}}\boldsymbol{f}(\boldsymbol{u})$ is the Hessian of $E(\boldsymbol{u})$ evaluated at $\boldsymbol{u}$.

7.2.2 The surrogate models: BSM and PMM

We consider as surrogate models those determined by the bridging scale method [56, 60] and the pseudo-spectral multiscale method [57]. These methods are similar and their overall objectives are to:

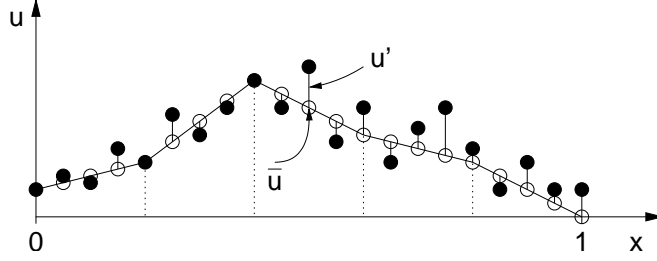1. Construct a coarse scale model from the MD model.

Figure 13: Illustration of the scale decomposition for BSM.

2. Solve the MD model only over a subdomain $\Omega_{MD} \subset \Omega$ and solve the coarse scale model in the complementary subdomain $\Omega_C = \Omega \setminus \Omega_{MD}$. One difficulty is then to develop proper interface conditions to reduce/eliminate spurious wave reflection at the interface of Ω_{MD} and Ω_C.

The starting point of BSM and PPM is based on the classical decomposition of scales (see *e.g.* [23]):

$$\boldsymbol{u} = \bar{\boldsymbol{u}} + \boldsymbol{u}', \quad \bar{\boldsymbol{u}} = \boldsymbol{P}\boldsymbol{u}, \quad \boldsymbol{u}' = \boldsymbol{Q}\boldsymbol{u} = (\boldsymbol{I} - \boldsymbol{P})\boldsymbol{u} \tag{77}$$

where $\bar{\boldsymbol{u}}$ and $\boldsymbol{u}'$ define the coarse-scale displacements and the fine-scale fluctuations, respectively, $\boldsymbol{P}$ is a general projection operator, and $\boldsymbol{I}$ is the identity matrix. One main difference between BSM and PPM is that $\bar{\boldsymbol{u}}$ is obtained in terms of piecewise linear functions in the case of BSM and of a spectral representation in the case of PPM.

Considering the subdomains Ω_{MD} and Ω_C, the solution $\boldsymbol{u}$ can be further decomposed into the following form:

$$\boldsymbol{u} = \begin{bmatrix} \boldsymbol{u}_{MD} \\ \boldsymbol{u}_C \end{bmatrix} = \begin{bmatrix} \bar{\boldsymbol{u}}_{MD} \\ \bar{\boldsymbol{u}}_C \end{bmatrix} + \begin{bmatrix} \boldsymbol{u}'_{MD} \\ \boldsymbol{u}'_C \end{bmatrix} \qquad \begin{array}{l} \text{in } \Omega_{MD} \\ \text{in } \Omega_C \end{array} \tag{78}$$

where $\boldsymbol{u}_{MD}$ and $\boldsymbol{u}_C$ are the parts of the solution in Ω_{MD} and in Ω_C, respectively. In essence, BSM and PMM consist in approximating the large scales $\bar{\boldsymbol{u}}_{MD} + \bar{\boldsymbol{u}}_C$ by constructing a coarse scale model over the whole domain Ω (see [60, 56, 57] for details) and by using $\bar{\boldsymbol{u}}_C$ to define the boundary conditions for the full MD model in Ω_{MD}. However, it is well known that such a coarse model may yield spurious wave reflection at the interface of the two domains. In order to alleviate this issue, BSM and PMM propose to calculate the fine scale components in Ω_C corresponding to those atoms that are within the cut-off radius of atoms in Ω_{MD}. Therefore, the vector $\boldsymbol{u}'_C$ is approximated by a vector, say $\boldsymbol{u}'_G$, that has zero entries, except at the position of these atoms "close" to the interface boundary. It follows that the surrogate models using BSM or PMM produce solutions in the form:

$$\tilde{\boldsymbol{u}} = \begin{bmatrix} \boldsymbol{u}_{MD} \\ \bar{\boldsymbol{u}}_C \end{bmatrix} \qquad \begin{array}{l} \text{in } \Omega_{MD} \\ \text{in } \Omega_C \end{array} \tag{79}$$

Once again, the readers are referred to [60, 56, 57] for the full description of the methods. Our main interest in the present work is to provide error estimates with respect to quantities of interest for the surrogate solutions $\tilde{\boldsymbol{u}}$.

37

7.2.3 Error estimates

The residual functional with respect to the MD problem can be written as

$$\mathcal{R}(\tilde{\boldsymbol{u}}, \boldsymbol{v}) = \int_0^T \boldsymbol{v}^T (\underbrace{\boldsymbol{M}\ddot{\tilde{\boldsymbol{u}}} - \boldsymbol{f}(\tilde{\boldsymbol{u}})}_{\boldsymbol{r}(\tilde{\boldsymbol{u}})}) dt = \int_0^T \sum_{i=1}^n \boldsymbol{v}_i \cdot \boldsymbol{r}_i(\tilde{\boldsymbol{u}}) dt \tag{80}$$

The local residual $\boldsymbol{r}_i$ simply indicates how the second Newton law fails to be satisfied at atom i. Given a quantity of interest $Q(\boldsymbol{u})$, the modeling error in $Q(\tilde{u})$ can be approximated by

$$Q(\boldsymbol{u}) - Q(\tilde{u}) \approx \mathcal{R}(\tilde{\boldsymbol{u}}, \boldsymbol{p}) = \int_0^T \sum_{i=1}^n \boldsymbol{p}_i \cdot \boldsymbol{r}_i(\tilde{u}) dt \tag{81}$$

where $\boldsymbol{p}$ is the dual solution associated with $Q(\boldsymbol{u})$. The computational domain is divided here into a partition $\{\Theta\}_{j=0}^k$, as indicated in Section 5. In the case of BSM, the subdomains are conveniently constructed from the coarse lattice used in the solution of the coarse scale model. We note that the error quantity can then be decomposed into local contributions either in time, η_t, or in space, η_j, as:

$$\eta_t = \sum_{i=1}^n \boldsymbol{p}_i \cdot \boldsymbol{r}_i(\tilde{u}) \qquad \eta_j = \int_0^T \sum_{i \in \Theta_j} \boldsymbol{p}_i \cdot \boldsymbol{r}_i(\tilde{u}) dt \tag{82}$$

and that the error can be rewritten in terms of these local contributions as:

$$Q(\boldsymbol{u}) - Q(\tilde{u}) \approx \mathcal{R}(\tilde{\boldsymbol{u}}, \boldsymbol{p}) = \int_0^T \eta_t dt = \sum_{j=0}^k \eta_j \tag{83}$$

We will show in the following example the distribution of the contributions η_i and the evolution of the contributions η_t.

7.2.4 Numerical example

The performance of the error estimator and of the local Goals algorithm is demonstrated here for the one-dimensional model problem studied in [56]. In this problem, $\Omega = [-2, 2]$, $\Omega_{MD} = [-0.35, 0.35]$, with atomic spacing $h_a = 0.005$. The atoms in domains Ω_{MD} and Ω_C are represented in black and red, respectively, in Fig. 14 and subsequent figures. The initial conditions are given by:

$$V_0(x_i) = 0, \qquad x_i \in \Omega \tag{84}$$

and

$$U_0(x_i) = \begin{cases} 0.005 \left(1 + 0.1 \cos(80\pi x_i)\right) \dfrac{e^{-100x_i^2} - e^{-6.25}}{1 - e^{-6.25}} & |x_i| \le 0.25 \\ 0 & \text{otherwise} \end{cases} \tag{85}$$
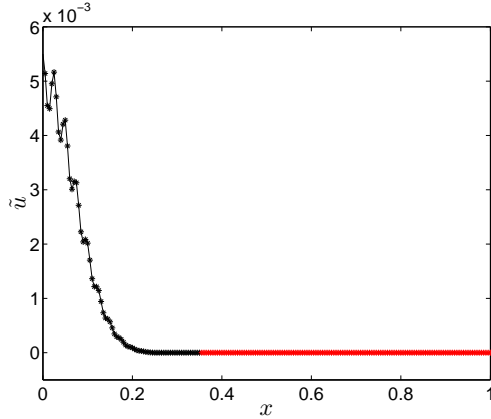
38

Figure 14: Initial displacement $U_0(x_i)$. The points in black represent atoms in Ω_{MD} while points in red denote atoms in Ω_C.

Furthermore, $m_i = 1$, $i = 1, \ldots, n$, and the interatomic forces are given by linear springs:

$$\boldsymbol{f}(\boldsymbol{u}) = \boldsymbol{K}\boldsymbol{u}, \qquad \boldsymbol{K} = \begin{bmatrix} -2 & 1 & & & \\ 1 & -2 & \ddots & & \\ & \ddots & \ddots & 1 & \\ & & 1 & -2 \end{bmatrix} \tag{86}$$

In the case of BSM, the coarse lattice is constructed by placing a coarse grid point at every p atom in Ω so that the coarse grid spacing $h_c = ph_a$; see Fig. 15. The time integration scheme is identical to that used by Wagner and Liu [60]. In this example, we suppose that we are interested in the locally averaged displacement:

$$Q(\boldsymbol{u}) = \frac{1}{\text{Card}\mathcal{M}} \sum_{i \in \mathcal{M}} u_i, \qquad \mathcal{M} = \{i : |x_i| \leq 0.0025\} \tag{87}$$

for which the strong form of the dual problem is determined as

$$\boldsymbol{M}\ddot{\boldsymbol{p}} - \left(\boldsymbol{f}'(\boldsymbol{u})\right)^T \boldsymbol{p} = \boldsymbol{0}, \qquad -\boldsymbol{M}\dot{\boldsymbol{p}}(T) = \boldsymbol{q}, \qquad \boldsymbol{p}(T) = \boldsymbol{0} \tag{88}$$

where $\boldsymbol{q}$ is the vector defined such that $Q(\boldsymbol{u}) = \boldsymbol{q}^T\boldsymbol{u}$. The dual problem is solved by integrating (88) backwards in time using a numerical scheme similar to that used in the forward time integration of the primal problem.

The first set of experiments deals with bridging scale method. The surrogate solution $\tilde{\boldsymbol{u}}$, the dual solution $\boldsymbol{p}$, and the local residuals $rr(\tilde{\boldsymbol{u}})$ are shown in Fig. 16 for four specific times. Observe how the dual solution propagates in time in the opposite direction to the primal solution. The dual solution indicates how the local residuals $\boldsymbol{r}(\tilde{\boldsymbol{u}})$ influence the error in the quantity of interest. In particular, it can be seen that, as the front moves left to right, the dual solution reduces to zero. This simply means that the sources of error introduced in those spatial regions in which the dual solution
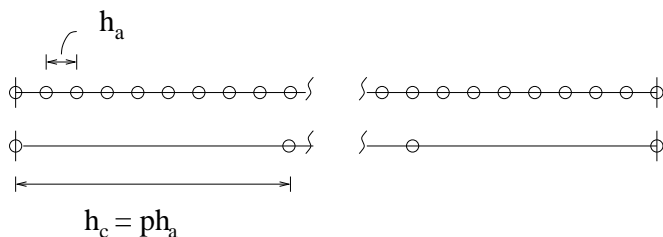
Figure 15: Schematic illustrating the construction of the coarse lattice on which the coarse scale displacements $\bar{\boldsymbol{u}}$ are computed (BSM).

is zero do not have enough time to propagate and pollute the quantity of interest. In the meantime, the local residuals become significant when the fine scale noise starts to move across the interface boundary. The combination of both effects implies that the major contributions to the error in the quantity of interest are generated during the time interval $0.35 \leq t \leq 0.90$ and in the subregion $0.35 \leq x \leq 0.5$ as shown in Fig. 17.

Since the sources of error, according to Fig. 17, are essentially created in the space intervals $[0.35, 0.5]$ and $[-0.5, -0.35]$ (by symmetry), we choose to enlarge Ω_{MD} to $[-0.5, 0.5]$ in a one adaptive step of the Goals algorithm. Fig. 18 displays the new error contributions along the pre-adapted solution errors for comparison. As clearly shown, the modeling error has been effectively eliminated. Note that the dual solution $\boldsymbol{p}$ in the present numerical experiment was computed using the fine scale model. A major task will be to construct adequate and reliable surrogate models for the dual problem.

We repeat the same experiments in the case of PMM. Here we only show the results of the adaptive algorithm by considering $\Omega_{MD} = [-0.5, 0.5]$, $[-0.4, 0.4]$, and $[-0.45, 0.45]$. Fig. 19 shows how the contribution to the errors are reduced by successive refinement of the model problem.

7.3   Random Heterogeneous Materials

We now show an application of the Local Goals algorithms to the analysis of the elastostatics of *random* multi-phase composite materials (see also [46]). In Section 7.3.1, we first define the model problem and notations. We then introduce a brief overview on the surrogate models and the estimation of modeling errors in Section 7.3.2 and present a specific example application to a two-phase composite material in Section 7.3.3.

7.3.1   Model Problem and Notations

We consider a material body, occupying an open and bounded domain $D \subset \mathbb{R}^d$, $d = 1, 2, 3$, with boundary $\partial D = \overline{\Gamma_u \cup \Gamma_t}$, $\Gamma_u \cap \Gamma_t = \emptyset$, $meas(\Gamma_t) > 0$, $meas(\Gamma_u) > 0$, Γ_u and Γ_t being portions of ∂D on which displacements and tractions are to be specified, respectively. The body is in static equilibrium under the action of deterministic applied forces $\boldsymbol{f} \in L^2(D)^d$, a surface traction $\boldsymbol{t} \in L^2(\Gamma_t)^{d-1}$, and a prescribed displacement $\boldsymbol{U} \in L^2(\Gamma_u)^d$ on Γ_u. We assume the body is composed of a multi-phase, composite, elastic material with highly oscillatory material properties. The geometrical features and material properties of its constituents are functions of a *random vector* $\boldsymbol{\omega} \in \Omega$,
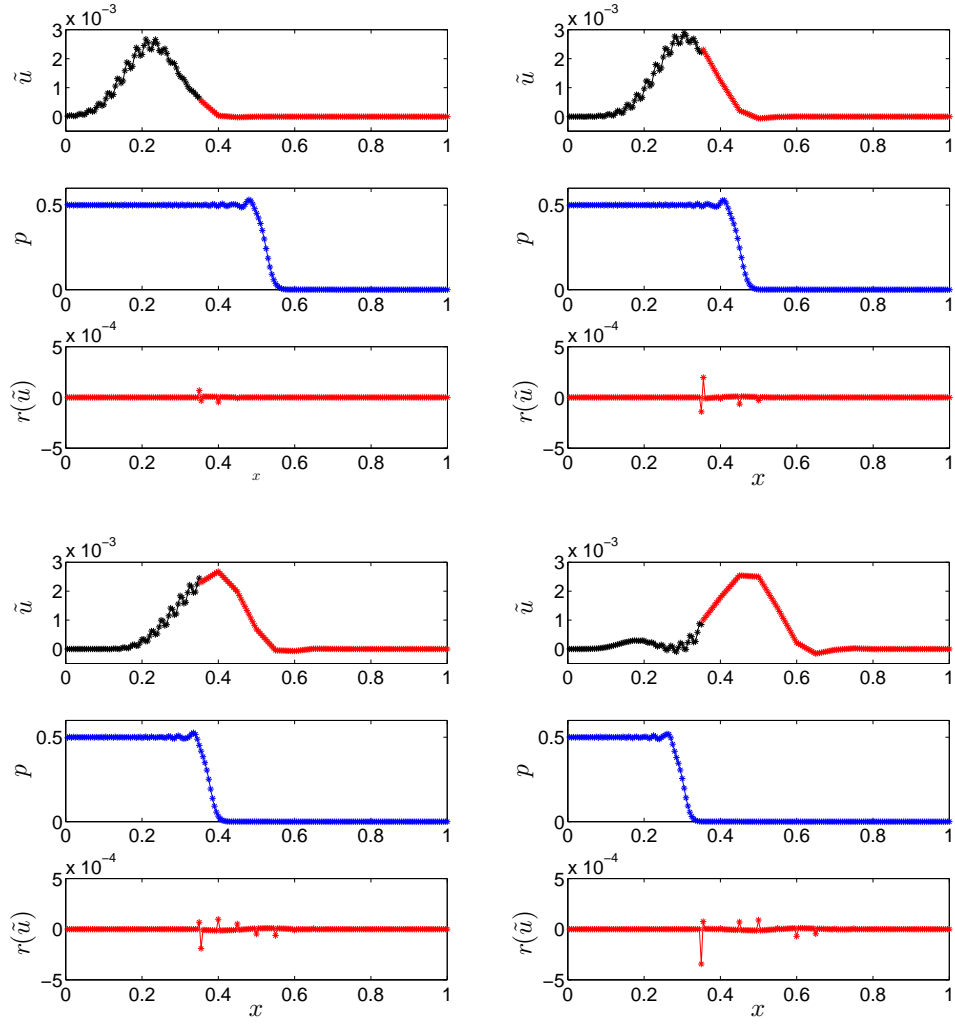
40

Figure 16: Time snapshots of the primal, dual, and force residual at $t = 45, 60, 75, 90$ (BSM).

where Ω denotes the collection of all possible realizations. The governing *probability distribution density function* $p : \Omega \longrightarrow [0, 1]$ is assumed to be known.

Let $\boldsymbol{u} = \boldsymbol{u}(\boldsymbol{x}, \boldsymbol{\omega})$ denote the random displacement vector field defined on $D \times \Omega$ and let $\boldsymbol{\nabla u}$ denote the spatial gradient. Then the Cauchy stress tensor $\boldsymbol{\sigma}(\boldsymbol{x}, \boldsymbol{\omega})$ satisfies $\boldsymbol{\sigma}(\boldsymbol{x}, \boldsymbol{\omega}) = \boldsymbol{E}(\boldsymbol{x}, \boldsymbol{\omega}) \boldsymbol{\nabla u}(\boldsymbol{x}, \boldsymbol{\omega})$, where $\boldsymbol{E}(\boldsymbol{x}, \boldsymbol{\omega})$ is the fourth order tensor of elasticities with components $E_{ijkl}(\boldsymbol{x}, \boldsymbol{\omega}) \in L^{\infty}(D, L^2(\Omega))^{d \times d}$. The standard symmetry and ellipticity conditions hold for a.e. $\boldsymbol{x} \in D$ and a.s. $\boldsymbol{\omega} \in \Omega$:

$$E_{ijkl}(\boldsymbol{x}, \boldsymbol{\omega}) = E_{jikl}(\boldsymbol{x}, \boldsymbol{\omega}) = E_{ijlk}(\boldsymbol{x}, \boldsymbol{\omega}) = E_{klij}(\boldsymbol{x}, \boldsymbol{\omega}).$$
$$\alpha_0 \xi_{ij} \xi_{ij} \leq E_{ijkl}(\boldsymbol{x}, \boldsymbol{\omega}) \xi_{ij} \xi_{kl} \leq \alpha_1 \xi_{ij} \xi_{ij}, \qquad \alpha_1 \geq \alpha_0 > 0.$$
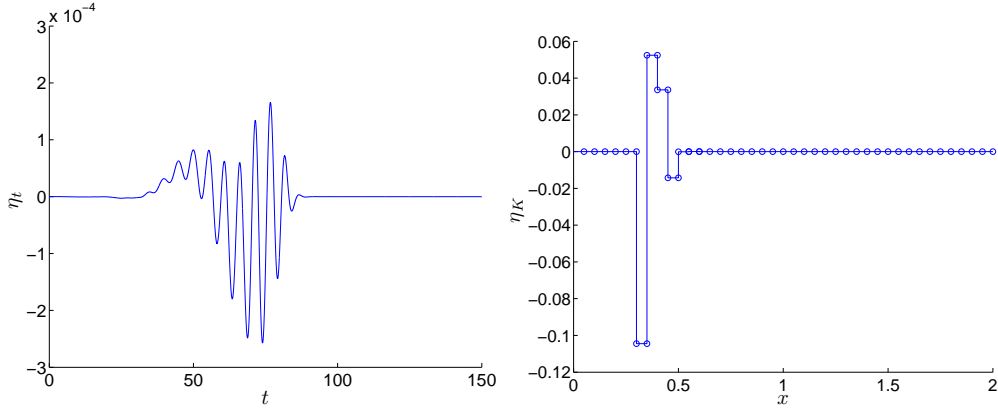
41

Figure 17: The temporal contribution to the error (left) and the spatial contribution (right) (BSM).
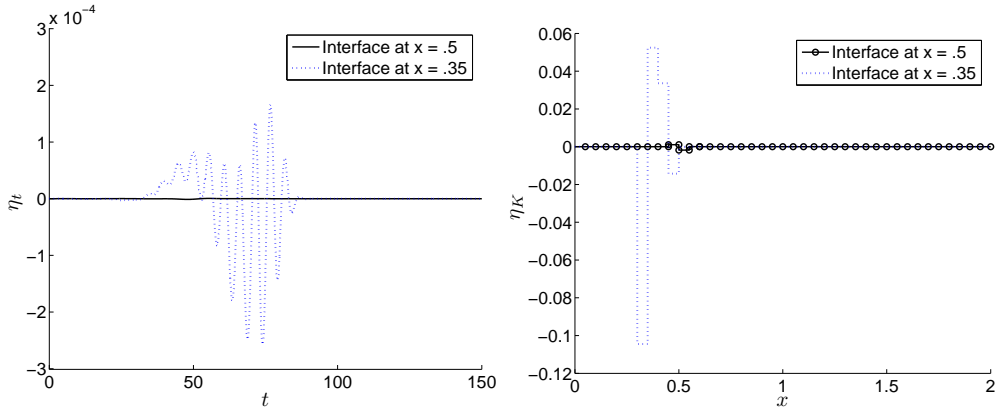

Figure 18: The temporal contribution to the error (left) and the spatial contribution (right) following model adaptivity (BSM).

We introduce a space of test functions V,

$$V = \left\{ \boldsymbol{v} \in H^1(D, L^2(\Omega)) : \ \boldsymbol{v}(\boldsymbol{x}, \boldsymbol{\omega}) = 0, \ \forall \boldsymbol{x} \in \Gamma_u, \ \boldsymbol{\omega} \in \Omega \right\}, \tag{89}$$

where $H^1(D, L^2(\Omega))$ is the Hilbert space,

$$H^1(D, L^2(\Omega)) = \left\{ \boldsymbol{v}(\boldsymbol{x}, \boldsymbol{\omega}) : \ \int_\Omega \int_D \left[\boldsymbol{\nabla v} : \boldsymbol{\nabla v} + \boldsymbol{v} : \boldsymbol{v} \right] p(\boldsymbol{\omega}) \, \mathrm{d}\boldsymbol{x} \, \mathrm{d}\boldsymbol{\omega} < \infty \right\}.$$

Having established the necessary notations and conventions, we now recall the variational formulation (9) of our linear, stochastic, elastostatics problem, where [46]:

$$F(\boldsymbol{v}) = \int_\Omega \int_D (\boldsymbol{f} : \boldsymbol{v}) \, p(\boldsymbol{\omega}) \, \mathrm{d}\boldsymbol{x} \, \mathrm{d}\boldsymbol{\omega} + \int_\Omega \int_{\Gamma_t} (\boldsymbol{t} : \boldsymbol{v}) \, p(\boldsymbol{\omega}) \, \mathrm{d}s \, \mathrm{d}\boldsymbol{\omega},$$

$$B(\boldsymbol{w}, \boldsymbol{v}) = \int_\Omega \int_D (\boldsymbol{E \nabla w} : \boldsymbol{\nabla v}) \, p(\boldsymbol{\omega}) \, \mathrm{d}\boldsymbol{x} \, \mathrm{d}\boldsymbol{\omega}, \tag{90}$$
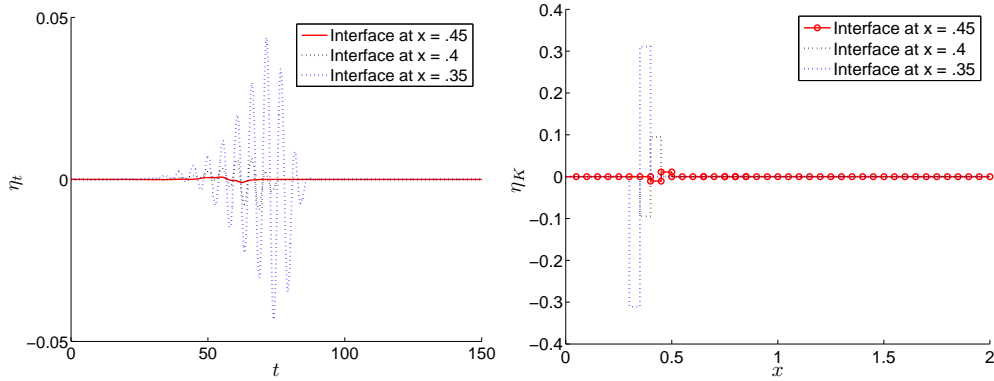
42

Figure 19: The temporal contribution to the error (left) and the spatial contribution (right) following model adaptivity (PMM).

where and $\boldsymbol{n}$ and $\boldsymbol{s}$ denote the unit normal and position vector on ∂D. Following the approach in Sections 1.2 and 2, we define the target of the analysis as a functional $Q(\cdot)$ of the solution $\boldsymbol{u}$.

7.3.2 Surrogate Models and Modeling Errors

To implement versions of the Goals algorithms, we compute a surrogate solution pair $(\boldsymbol{u}_0, \boldsymbol{p}_0)$ of (18), where the bilinear form $B_0(\cdot, \cdot)$ is obtained by first computing the statistical mean $\bar{\boldsymbol{E}}(\boldsymbol{x})$ of $\boldsymbol{E}(\boldsymbol{x}, \boldsymbol{\omega})$ and by then using standard homogenization methods or classical Hashin-Shtrikman bounds [22] to obtain the *deterministic, homogeneous,* elasticity tensor $\boldsymbol{E}_0$. Thus,

$$B_0(\boldsymbol{w}, \boldsymbol{v}) = \int_\Omega \int_D (\boldsymbol{E}_0 \boldsymbol{\nabla w} : \boldsymbol{\nabla v}) \, p(\boldsymbol{\omega}) \, \mathrm{d}\boldsymbol{x} \, \mathrm{d}\boldsymbol{\omega}. \tag{91}$$

The incurred modeling errors are denoted as $\boldsymbol{e}_0(\boldsymbol{x}, \boldsymbol{\omega}) = \boldsymbol{u}(\boldsymbol{x}, \boldsymbol{\omega}) - \boldsymbol{u}_0(\boldsymbol{x}, \boldsymbol{\omega})$ and $\boldsymbol{\varepsilon}_0(\boldsymbol{x}, \boldsymbol{\omega}) = \boldsymbol{p}(\boldsymbol{x}, \boldsymbol{\omega}) - \boldsymbol{p}_0(\boldsymbol{x}, \boldsymbol{\omega})$. The corresponding residual functionals (12) and (16) reduce to [46]:

$$\begin{aligned}
\mathcal{R}(\boldsymbol{u}_0, \boldsymbol{v}) &= - \int_\Omega \int_D (\boldsymbol{E} \mathcal{I}_0 \boldsymbol{\nabla u}_0 \cdot \boldsymbol{\nabla v}) \, p(\boldsymbol{\omega}) \, \mathrm{d}\boldsymbol{x} \, \mathrm{d}\boldsymbol{\omega}, \\
\overline{\mathcal{R}}(\boldsymbol{p}_0, \boldsymbol{z}) &= - \int_\Omega \int_D (\boldsymbol{E} \mathcal{I}_0 \boldsymbol{\nabla z} \cdot \boldsymbol{\nabla p}_0) \, p(\boldsymbol{\omega}) \, \mathrm{d}\boldsymbol{x} \, \mathrm{d}\boldsymbol{\omega},
\end{aligned} \tag{92}$$

where $\mathcal{I}_0(\boldsymbol{x}, \boldsymbol{\omega}) = \boldsymbol{I} - \boldsymbol{E}^{-1} \boldsymbol{E}_0$ denotes the *deviation tensor.* We can now call upon Corollary 1 to establish the error in the quantity of interest,

$$\mathcal{E}(\boldsymbol{u}_0) = \mathcal{R}(\boldsymbol{u}_0; \boldsymbol{p}_0) + \frac{1}{2}(\mathcal{R}(\boldsymbol{u}_0, \boldsymbol{\varepsilon}_0) + \overline{\mathcal{R}}(\boldsymbol{p}_0, \boldsymbol{e}_0))) + \Delta_2(\boldsymbol{u}_0, \boldsymbol{p}_0, \boldsymbol{e}_0, \boldsymbol{\varepsilon}_0)$$

Ignoring the higher order term $\Delta_2(\boldsymbol{u}_0, \boldsymbol{p}_0, \boldsymbol{e}_0, \boldsymbol{\varepsilon}_0)$, yields the estimate,

$$\mathcal{E}(\boldsymbol{u}_0) \approx \mathcal{R}(\boldsymbol{u}_0; \boldsymbol{p}_0) + \frac{1}{2}(\mathcal{R}(\boldsymbol{u}_0, \boldsymbol{\varepsilon}_0) + \overline{\mathcal{R}}(\boldsymbol{p}_0, \boldsymbol{e}_0))) \tag{93}$$

The last two terms in the RHS of (93) are generally intractable and further steps need to be taken to derive a computable estimate of the error. We here introduce an example of an estimator derived in [46] which is used in the example problem in Section 7.3.3:

$$\boxed{\mathcal{E}(\boldsymbol{u}_0) \approx \eta_{\mathrm{est,upp}} = \mathcal{R}(\boldsymbol{u}_0, \boldsymbol{p}_0) + \frac{1}{4}(\eta_{\mathrm{upp}}^+)^2 - \frac{1}{4}(\eta_{\mathrm{upp}}^-)^2,}$$

where

$$\eta_{\mathrm{upp}}^{\pm} = \sqrt{\int_{\Omega} \int_{D} \boldsymbol{E}\mathcal{I}_0 \boldsymbol{\nabla}(\boldsymbol{u}_0 \pm \boldsymbol{p}_0) : \mathcal{I}_0 \boldsymbol{\nabla}(\boldsymbol{u}_0 \pm \boldsymbol{p}_0) \, p(\boldsymbol{\omega}) \, \mathrm{d}\boldsymbol{x} \, \mathrm{d}\boldsymbol{\omega}}.$$

The Goals algorithm provides with two approaches to reduce the error $\mathcal{E}(\boldsymbol{u}_0)$ and compute enhanced solutions $(\tilde{\boldsymbol{u}}, \tilde{\boldsymbol{p}})$ of $(\boldsymbol{u}_0, \boldsymbol{p}_0)$: the Local or the Global Goals version (see Section 5). In either case, we use the estimator $\tilde{\eta}_{\mathrm{est}}$, derived from (45), to assess the error in the quantity of interest of the enhanced solutions,

$$\mathcal{E}(\tilde{\boldsymbol{u}}) \approx \tilde{\eta}_{\mathrm{est}} = \mathcal{R}(\boldsymbol{u}_0, \tilde{\boldsymbol{p}}) + Q(\boldsymbol{u}_0) - Q(\tilde{\boldsymbol{u}}).$$

7.3.3 Numerical Example

For the base problem, we consider a two-phase composite material consisting of isotropic, linearly elastic constituents. Cylindrical inclusions account for 30 percent of the volume and have been randomly dispersed in the matrix material, as depicted in Fig. 20. The structure is subjected to a traction $\boldsymbol{t}$ at the top and has prescribed zero displacements at the base $y = 0$. The Young's modulus and Poisson ratio of the matrix material are deterministic and given by $E_{\mathrm{m}} = 5$ GPa and $\nu_{\mathrm{m}} = 0.345$. The material properties of the inclusions, however, are functions of the random vector $\boldsymbol{\omega} = \{\omega_1, \omega_2\} \in (0, 1) \times (0, 1)$, such that:

$$E_{\mathrm{incl}}(\boldsymbol{\omega}) \quad = E_{\mathrm{incl}}(\omega_1) \quad = 110\mathrm{GPa} + 20\mathrm{GPa} \times \omega_1,$$

$$\nu_{\mathrm{incl}}(\boldsymbol{\omega}) \quad = \nu_{\mathrm{incl}}(\omega_2) \quad = 0.28 + 0.4 \times \omega_2,$$

We assume that ω_1 and ω_2 are statistically independent which implies that $p(\boldsymbol{\omega}) = p_1(\omega_1) \, p_2(\omega_2)$. We additionally assume that $p_i(\omega_i)$, $i = 1, 2$, are *truncated Gaussian distribution density functions*,

$$p_i(\omega_i) = 2 \frac{A}{\sqrt{2\pi}} \, e^{-(2\omega_i - 1)^2/2\pi}, \quad i = 1, 2$$

$$A = 2 \left[\mathrm{erf}\left(\frac{1}{\sqrt{2\pi}}\right) - \mathrm{erf}\left(-\frac{1}{\sqrt{2\pi}}\right) \right]^{-1}$$

In this example, our target $Q(\boldsymbol{u})$ is the statistical average of the average strain ε_{yy} over a small circular area D_Q near the support of the structure, with a radius $r = 0.017\mathrm{m}$ (see Fig. 20).

We establish the surrogate problem (18) by computing the average of the Hashin-Shtrikman upper and lower bounds [22] of the material coefficients in the base model.
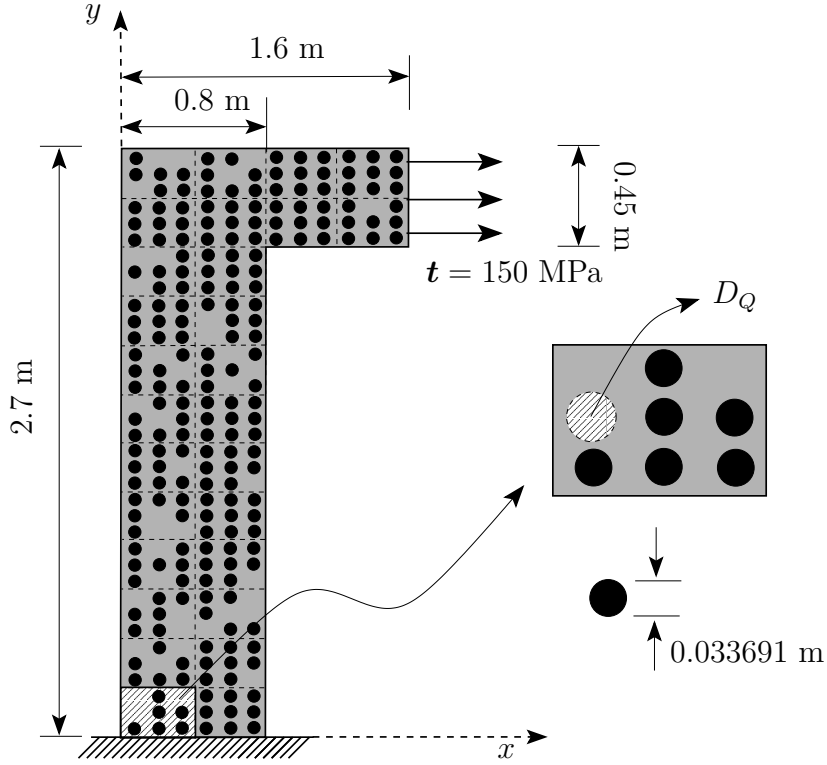
44

Figure 20: A structural component constructed from a two-phase composite material in equilibrium under the action of applied stress t and prescribed zero displacements at $y = 0$.

Using these averaged coefficients, we construct a a surrogate $\boldsymbol{E}_0$ whose coefficients are obviously *homogeneous and deterministic*. It is easy to show [47] that with the current choice of $Q(\boldsymbol{u})$ the surrogate solutions $(\boldsymbol{u}_0, \boldsymbol{p}_0)$ are also deterministic functions. In Fig. 21, the strain field ε_{yy}^0 is shown which is obtained by using overkill finite element (FE) approximations of $(\boldsymbol{u}_0, \boldsymbol{p}_0)$ (All FE computations are performed with the FE code ProPHLEX [2]).

For comparison, the base solution $\boldsymbol{u}(\boldsymbol{x}, \omega)$ has also been computed by using overkill Monte Carlo and FE approximations and the statistical average of the resulting strain field $\varepsilon_{yy}(\boldsymbol{x}, \omega)$ is shown in Fig. 22, where the area of interest around D_Q has been magnified. In Table 1, the relative error in the quantity of interest and the effectivity indices of the estimate $\eta_{\text{est,upp}}$ is given. The relative error appears to be large, but with a reasonable effectivity of 122 percent, the estimator $\eta_{\text{est,upp}}$ provides a fairly accurate assessment of the error.

To reduce the error, we perform two separate series of local enhancements. In one series, we employ the Local Goals algorithm, while the global Goals is used in a second series. In Table 2, the relative errors and the effectivity indices of the error estimator $\tilde{\eta}_{\text{est}}$ are listed for three steps of both approaches. Also, in Figures 23 and 24, the statistical averages of the enhanced strain fields $\tilde{\varepsilon}_{yy}$ are shown that are obtained after the first and third step, respectively. In these figures, the boundary of the domain of

45

influence ∂D_L is highlighted red.

As expected (see Remark 2), the results in Table 2 reveal that, although the Global Goals algorithm requires solving a larger problem, the rate of decrease in the error in the target quantity is more pronounced with this approach. In both approaches, the estimator $\tilde{\eta}_{\text{est}}$ exhibits good accuracy with effectivity indices close to unity. For the Global Goals version, the effectivity is slightly worse, but this is due to the fact that the error has been reduced to much smaller values. In most applications, however, the estimators will lose some accuracy as the error becomes very small.

$\mathcal{E}(\boldsymbol{u}_0)/Q(\boldsymbol{u})$	$\eta_{\text{est,upp}}/\mathcal{E}(\boldsymbol{u}_0)$
0.73	1.22

Table 1: Relative error and effectivity index of the estimator $\eta_{\text{est,upp}}$.

	Local Goals		Global Goals	
Step No.	$\mathcal{E}(\tilde{\boldsymbol{u}})/Q(\boldsymbol{u})$	$\tilde{\eta}_{\text{est}}/\mathcal{E}(\tilde{\boldsymbol{u}})$	$\mathcal{E}(\tilde{\boldsymbol{u}})/Q(\boldsymbol{u})$	$\tilde{\eta}_{\text{est}}/\mathcal{E}(\tilde{\boldsymbol{u}})$
1	0.61	1.07	0.20	1.31
2	0.61	1.10	0.15	1.49
3	0.56	1.08	0.13	1.40

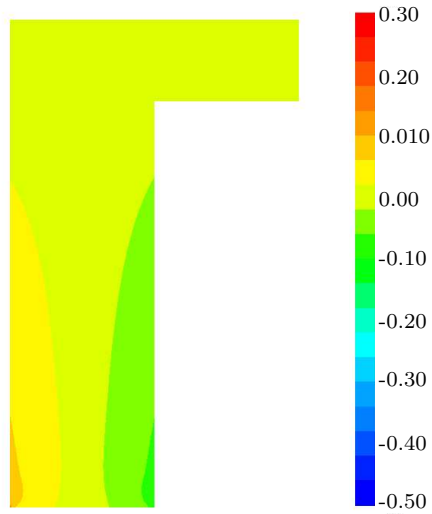Table 2: Relative error and estimator effectivity for the locally enhanced problems.

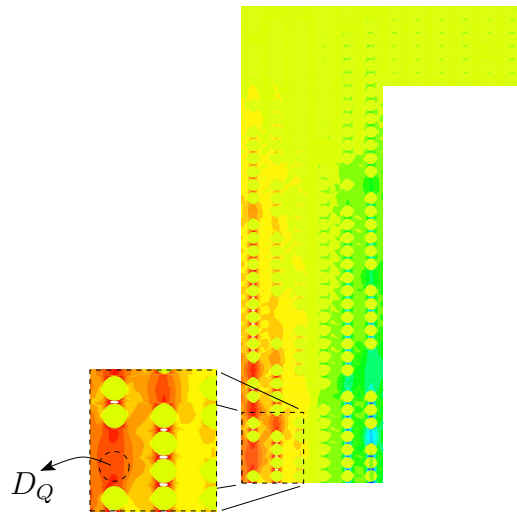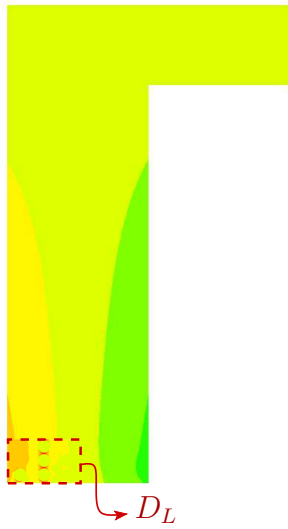Figure 21: Strain field ε_{yy}^0 for the deterministic surrogate problem.

Figure 22: Mean value of the strain field ε_{yy} for the base problem.
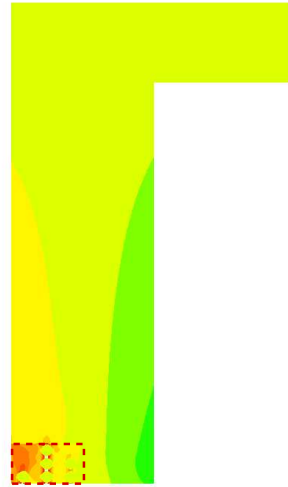
(a) Local Goals   (b) Global Goals

Figure 23: Mean values of the strain field $\tilde{\varepsilon}_{yy}$ after the first step of local enhancement using the Local and Global Goals algorithm.
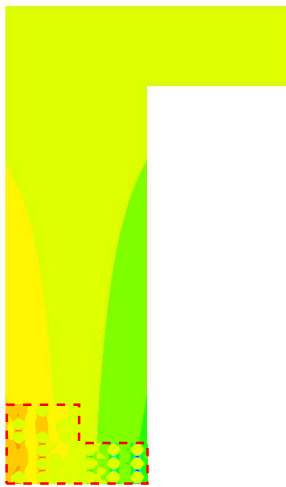

(a) Local Goals   (b) Global Goals
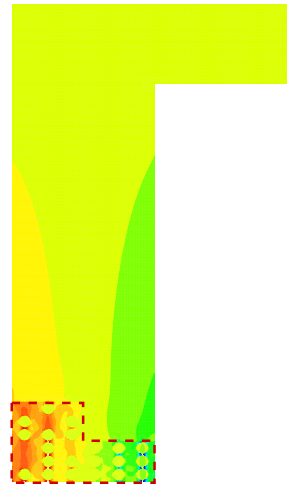
Figure 24: Mean values of the strain field $\tilde{\varepsilon}_{yy}$ after the third step of local enhancement using the Local and Global Goals algorithm.

7.4 Quantum Mechanics Models and the QM-Molecular Dynamics Interface

Our goal here is to briefly demonstrate how classical quantum mechanics itself has been the springboard for creating numerous reduced models of various structures and that these can also be viewed as surrogate to a more general base system. Moreover, we also describe how the framework developed thusfar provides a basis for characterizing the interface of QM models with those of molecular dynamics. A more detailed exposition of these ideas is to be the subject of a future paper.

We focus on a nonrelativistic molecular system consisting of M nuclei and N electrons interacting through Coulombic forces. The Hamiltonian for such systems is:

$$
\begin{aligned}
H = &-\frac{\hbar^2}{2m}\sum_{i=1}^{N}\Delta_{\boldsymbol{r}_i} - \frac{\hbar^2}{2}\sum_{K=1}^{M}\frac{1}{M_K}\Delta_{\boldsymbol{R}_K} - \sum_{i=1}^{N}\sum_{K=1}^{M}\frac{Z_K e^2}{r_{Ki}} \\
&+ \sum_{K>L}\frac{Z_K Z_L e^2}{R_{KL}} + \sum_{i>j}\frac{e^2}{r_{ij}}
\end{aligned}
\tag{94}
$$

where $\hbar$ is Planck's constant, m the electron mass, $\Delta_{\boldsymbol{r}_i}$ and $\Delta_{\boldsymbol{R}_K}$ the Laplacians in the $\boldsymbol{r}_i$ and $\boldsymbol{R}_K$ coordinates, $\boldsymbol{r}_i$ and $\boldsymbol{R}_K$ being the position vectors to electron i and nuclei K, respectively, M_K is the mass of nuclei K, e the electron charge, eZ_K is the charge of nuclei K, $r_{Ki} = |\boldsymbol{r}_i - \boldsymbol{R}_K|$, $R_{KL} = |\boldsymbol{R}_K - \boldsymbol{R}_L|$, and $r_{ij} = |\boldsymbol{r}_i - \boldsymbol{r}_j|$, $1 \le K, L \le M$, $1 \le i, j \le N$. Ignoring electron spin coordinates for simplicity in notation, the time-independent Schrödinger equation for this molecular system can be written,

$$
B(\Psi, \Phi) = \langle\Phi, H\Psi\rangle - E_T\langle\Phi, \Psi\rangle = 0, \qquad \forall \Phi \in \mathcal{H}_N
\tag{95}
$$

where Ψ is the wave function, dependent on the $3N$ vector $\boldsymbol{r} = (\boldsymbol{r}_1, \boldsymbol{r}_2, \ldots \boldsymbol{r}_N)$ and the $3M$ vector $\boldsymbol{R} = (\boldsymbol{R}_1, \boldsymbol{R}_2, \ldots \boldsymbol{R}_M)$,

$$
\begin{aligned}
B(\Psi, \Phi) = \ &\frac{\hbar^2}{2m}\sum_{i=1}^{N}\int_{\mathbb{R}^3}\int_{\mathbb{R}^{3M}}\boldsymbol{\nabla}_{\boldsymbol{r}_i}\Phi^* \cdot \boldsymbol{\nabla}_{\boldsymbol{r}_i}\Psi \, \mathrm{d}r_i \, \mathrm{d}^{3M}R \\
&+ \frac{\hbar^2}{2}\sum_{K=1}^{M}\int_{\mathbb{R}^3}\int_{\mathbb{R}^{3N}}\boldsymbol{\nabla}_{\boldsymbol{R}_K}\Phi^* \cdot \boldsymbol{\nabla}_{\boldsymbol{R}_K}\Psi \, \mathrm{d}R_K \, \mathrm{d}^{3N}r \\
&+ \int_{\mathbb{R}^{3N}}\int_{\mathbb{R}^{3M}}\Phi^*\left(V_{eM}(\boldsymbol{r}, \boldsymbol{R}) + V_{MM}(\boldsymbol{R}) + V_{ee}(\boldsymbol{r})\right)\Psi \, \mathrm{d}^{3N}r \, \mathrm{d}^{3M}R \\
&- E_T\langle\Phi, \Psi\rangle.
\end{aligned}
\tag{96}
$$

Here, V_{eM}, V_{MM}, and V_{ee} are the third, fourth, and fifth (potential) terms on the right-hand-side of (94), respectively, E_T is the total energy,

$$
\langle\Phi, \Psi\rangle = \int_{\mathbb{R}^{3N}}\int_{\mathbb{R}^{3M}}\Phi^*(\boldsymbol{r}, \boldsymbol{R})\Psi(\boldsymbol{r}, \boldsymbol{R}) \, \mathrm{d}^{3M}R \, \mathrm{d}^{3N}r,
$$

and $\mathcal{H}_N$ is the subspace of normalized functions,

$$
\mathcal{H}_N = \left\{\Phi \in \mathcal{H} : \|\Phi\| = 1\right\},
\tag{97}
$$

where $\|\Phi\|^2 = \int_{\mathbb{R}^{3N}} \int_{\mathbb{R}^{3M}} \Phi^* \Phi \, \mathrm{d}^{3M} R \, \mathrm{d}^{3N} r$, with

$$\mathcal{H} = \left\{ \Phi = \Phi(\boldsymbol{r}, \boldsymbol{R}) | \ \Phi \in H^1(\mathbb{R}^{3N} \times \mathbb{R}^{3M}; \mathbb{C}) \cap L_a^2(\mathbb{R}^{3N} \times \mathbb{R}^{3M}) \right\}, \qquad (98)$$

$L_a^2(\cdot)$ being the space of complex-valued L^2-functions, anti-symmetric with respect to the election positions in respect of the Pauli principle.

The *primal base problem* consists of finding the pairs $(\Psi, E_T) \in \mathcal{H}_N \times \mathbb{R}$ such that:

$$\boxed{B(\Psi, \Phi) = 0 = \langle \Phi, H\Psi \rangle - E_T \langle \Phi, \Psi \rangle, \qquad \forall \Phi \in \mathcal{H}_N.} \qquad (99)$$

Since H is Hermitian, E_T is real.

Let us take the ground state energy $E_g = \min E_T$ as our quantity of interest,

$$Q(\Psi) = E_g = \inf_{\Phi \in \mathcal{H}_N} \langle \Phi, H\Phi \rangle. \qquad (100)$$

Then the dual problem is to find $P \in \mathcal{H}_N$ such that

$$\boxed{B(\Phi, P) = \langle \Phi, H\Psi \rangle + \langle \Psi, H\Phi \rangle, \qquad \forall \Phi \in \mathcal{H}_N.} \qquad (101)$$

Clearly,
$$0 = B(\Psi, P) = \langle \Psi, H\Psi \rangle + \langle \Psi, H\Psi \rangle = \langle \Psi, H\Psi \rangle - E_T \langle \Psi, \Psi \rangle,$$

so that $E_T = \langle \Psi, H\Psi \rangle / \langle \Psi, \Psi \rangle$, as expected.

7.4.1 Surrogate Models via the Born-Oppenheimer Approximation

The classical Born-Oppenheimer approximation is based on the assumption that the nuclei, being much more massive than the electrons, can be treated as fixed points for the purpose of computing the electronic structure (the ground state energy) of the system. In particular, for the electron calculations, the nuclei positions $\boldsymbol{R} = (\boldsymbol{R}_1, \boldsymbol{R}_2, \ldots, \boldsymbol{R}_M)$ are treated as parameters and the wave function decomposes as follows:

$$\Psi(\boldsymbol{r}, \boldsymbol{R}) = \Psi_e(\boldsymbol{r}; \boldsymbol{R}) \, \chi(\boldsymbol{R}),$$

Ψ_e being the electronic part, depending parametrically on $\boldsymbol{R}$, and $\chi(\boldsymbol{R})$ the contribution to the wave function from the nuclei system. Schrödinger's equation for the electronic contribution is then

$$H_{\mathrm{elec}} \Psi_e(\boldsymbol{r}; \boldsymbol{R}) = E_{\mathrm{elec}}(\boldsymbol{R}) \Psi_e(\boldsymbol{r}; \boldsymbol{R}),$$

where
$$H_{\mathrm{elec}} = T_e(\boldsymbol{r}) + V_{eM}(\boldsymbol{r}; \boldsymbol{R}) + V_{MM}(\boldsymbol{R}),$$

$T_e(\boldsymbol{r})$ being the electron kinetic energy and $E_{\mathrm{elec}}(\boldsymbol{R})$ is the energy of the electron system, dependent now only on $\boldsymbol{R}$. The energy for the total molecular system is thus (neglecting the nuclei kinetic energy):

$$E_T(\boldsymbol{R}^*) = \inf_{\boldsymbol{R} \in \mathbb{R}^{3M}} \left\{ E_{\mathrm{elec}}(\boldsymbol{R}) + V_{MM}(\boldsymbol{R}) \right\}. \qquad (102)$$

Let $\chi(\boldsymbol{R})$ denote the nuclear wave function in a Born-Oppenheimer approximation; *e.g.*

$$H_{\mathrm{nuc}}(\boldsymbol{R})\,\chi(\boldsymbol{R}) = (T_M(\boldsymbol{R}) + E_{\mathrm{elec}}(\boldsymbol{R}) + V_{MM}(\boldsymbol{R}))\,\chi(\boldsymbol{R}) = \tilde{E}_T\,\chi(\boldsymbol{R}),$$

$\tilde{E}_T$ being the approximate total energy. Let Ψ_0 denote the wave function for the full surrogate system: $\Psi_0(\boldsymbol{r},\boldsymbol{R}) = \Psi_e(\boldsymbol{r};\boldsymbol{R})\,\chi(\boldsymbol{R})$. Then the error in the quantity of interest is

$$
\mathcal{E}(\Psi_0) = \mathcal{R}(\Psi_0; P) = \int_{\mathbb{R}^{3N}} \int_{\mathbb{R}^{3M}} P^*(\boldsymbol{r},\boldsymbol{R})\big[H_{\mathrm{nuc}}(\boldsymbol{R}) \\
+ H_{\mathrm{elec}}(\boldsymbol{r};\boldsymbol{R}) - E_T\big]\,\Psi_0(\boldsymbol{r};\boldsymbol{R})\,\mathrm{d}^{3N}r\,\mathrm{d}^{3M}R \tag{103}
$$

In the event that $T_M(\boldsymbol{R})$ is omitted and the influence function P can be decomposed into product functions $P(\boldsymbol{r},\boldsymbol{R}) = P_r(\boldsymbol{r})P_R(\boldsymbol{R})$, the estimate (103) simplifies to

$$\mathcal{E}(\Psi_0) \approx \int_{\mathbb{R}^{3N}} \int_{\mathbb{R}^{3M}} P^*(\boldsymbol{r},\boldsymbol{R})\big[\tilde{E}_T + E_{\mathrm{elec}}(\boldsymbol{R}) - E_T\big]\,\Psi_0(\boldsymbol{r};\boldsymbol{R})\,\mathrm{d}^{3N}r\,\mathrm{d}^{3M}R. \tag{104}$$

Molecular Dynamics. The transition from quantum mechanics to the Newtonian mechanics description of the dynamics of molecular systems is justified by the Bohr correspondence principle, characterized by Born [9] as follows: *"Judged by the test of experience, the laws of classical physics have brilliantly justified themselves in all processes of motion, macroscopic and microscopic, down to the motion of atoms as a whole (kinetic theory of matter). It must therefore be laid down, as an unconditionally necessary postulate, that the new mechanics [circa 1923], supposed still unknown, must in all problems reach the same results as the classical mechanics. In other words, it must be demonstrated that, for the limiting cases of large masses and of orbits of large dimension, the new mechanics passes over into the classical mechanics"*. This principle is very compatible with models based on the Born-Oppenheimer approximation. In place of the exterior optimization problem (102) we can use the molecular dynamics system,

$$M_K \ddot{\boldsymbol{R}}_K(t) + \frac{\partial U(\boldsymbol{R})}{\partial \boldsymbol{R}_K} = \boldsymbol{0}, \quad 1 \leq K \leq M, \tag{105}$$

with periodic boundary conditions in $\mathbb{R}^3$ and with appropriate initial conditions. Here U is the potential energy of the molecular system. The total energy is

$$E^{MD} = \sum_{K=1}^{M} \frac{\boldsymbol{P}_K \cdot \boldsymbol{P}_K}{2M_K} + U(\boldsymbol{R}),$$

with $\boldsymbol{P}_K = M_K \dot{\boldsymbol{R}}_K$ the momentum vector at site K. At equilibrium configurations, $\boldsymbol{R}^0$,

$$\frac{\partial U(\boldsymbol{R}^0)}{\partial \boldsymbol{R}_K} = \boldsymbol{0}, \tag{106}$$

and $E^{MD} = U(\boldsymbol{R}^0)$. A surrogate problem then involves introducing the pair $(\Psi^0, \tilde{E}_T) = (\chi^0(\boldsymbol{R}^0), E^{MD}(\boldsymbol{R}^0))$ where

$$B_0(\chi^0, \Phi) = \langle \Phi, H_{\mathrm{nuc}}(\boldsymbol{R}^0) \chi^0 \rangle - E^{MD}(\boldsymbol{R}^0)\langle \Phi, \chi^0 \rangle = 0, \qquad \forall \Phi \in \tilde{\mathcal{H}}, \tag{107}$$

51

with $\tilde{\mathcal{H}} = \{\Phi \in H^1(\mathbb{R}^{3M}, \mathbb{C}) \cap L^2_a(\mathbb{R}^{3M}), \|\Phi\|^2 = \langle \Phi, \Phi \rangle = 1\}$, $E^{MD}(\boldsymbol{R}^0) = U(\boldsymbol{R}^0)$, and now $\langle \Phi, \chi \rangle = \int_{\mathbb{R}^{3M}} \Phi^* \chi \mathrm{d}^{3M} R$. At this point χ^0 can be an arbitrary function in $\mathcal{H}$. The generation of a sequence of surrogate solutions χ^0 that systematically reduce the modeling error satisfying (107) is an open problem.

Approximate Potentials. The potential energy U in the MD models (105) or (106) can be identified with the ground state energy of the molecular system. Thus,

$$U(\boldsymbol{R}) \quad = E_T(\boldsymbol{R}) - \frac{1}{2} \sum_{K=1}^{M} M_K \dot{\boldsymbol{R}}_K \cdot \dot{\boldsymbol{R}}_K$$

$$= E_{\mathrm{elec}}(\boldsymbol{R}) + V_{MM}(\boldsymbol{R}),$$

so that the forces on a nuclei set are

$$\boldsymbol{F}_K(\boldsymbol{R}) \quad = -\frac{\partial U(\boldsymbol{R})}{\partial \boldsymbol{R}_K}$$

$$\approx \frac{\partial E_{\mathrm{elec}}(\boldsymbol{R})}{\partial \boldsymbol{R}_K} - \sum_{K>L}^{M} \frac{e^2 Z_K Z_L (\boldsymbol{R}_K - \boldsymbol{R}_L)}{R_{KL}^3},$$

$1 \leq K \leq M$. One can therefore proceed with an MD model calculation using electron ground state energies or an approximation if E_{elec} is in hand. There is a large literature on methods for approximating E_{elec} dating back over half a century. We provide two classical examples in concluding this subsection.

Hartree-Fock Model The classical Hartree-Fock model [21, 17] of the electronic structure of nonrelativistic systems is based on the Born-Oppenheimer approximation described earlier. The idea is to represent the electronic wave function as the Slater determinant,

$$\Psi_e^{HF}(\boldsymbol{r}; \boldsymbol{R}) \quad = \frac{1}{\sqrt{N!}} \sum_{\sigma} (-1)^{|\sigma|} \prod_{i=1}^{N} \varphi_{\sigma(i)}(\boldsymbol{r}_i)$$

$$= \frac{1}{\sqrt{N!}} \det(\varphi_i(\boldsymbol{r}_j)),$$

the sum taken over all permutations σ of the indices, $|\sigma|$ being the signature of σ, and the φ_i being so-called molecular orbitals. The functional

$$E^{HF}(\boldsymbol{\Phi}; \boldsymbol{R}) = \langle \Psi_e^{HF}, H_{\mathrm{elec}} \Psi_e^{HF} \rangle \approx E_{\mathrm{elec}}$$

is the Hartree-Fock representation of the energy of the electronic system, and $\boldsymbol{\Phi} = (\varphi_1(\boldsymbol{r}_1), \varphi_2(\boldsymbol{r}_2), \ldots, \varphi_N(\boldsymbol{r}_N))$.

Electronic calculations are usually based on Ritz approximations of the orbitals of the form

$$\varphi_i^h(\boldsymbol{r}_i) = \sum_{k=1}^{P} c_{ik} \, \chi_k(\boldsymbol{r}_i),$$

where the χ_k are linearly independent basis functions and

$$\mathrm{span} \left\{ \prod_{i=1}^{N} \{\chi_k(\boldsymbol{r}_i)\} \right\} = \mathcal{H}^{NP} \subset \mathcal{H}.$$

52

We then compute

$$E_{\text{elec}} \approx E_{\text{elec}}^h(\boldsymbol{R}) = \inf_{\boldsymbol{\Phi}^h \in \mathcal{H}^{NP}} E^{HF}(\boldsymbol{\Phi}^h; \boldsymbol{R}).$$

Density Functional Theory. A more popular approach toward computing approximations to E_{elec} is to use Density Functional Theory [44]. Then

$$E_{\text{elec}} = \inf_{\rho \in K} \mathcal{E}^{DFT}(\rho),$$

where, for the Thomas-Fermi Theory, for example,

$$
\begin{aligned}
\mathcal{E}^{DFT}(\rho) &= c_o \int_{\mathbb{R}^3} |\nabla \sqrt{\rho}|^2 \, \mathrm{d}r + c_1 \int_{\mathbb{R}^3} \rho^{5/3} \mathrm{d}r \\
&+ \frac{1}{2} \int_{\mathbb{R}^3} \int_{\mathbb{R}^3} \frac{\rho \mathbf{x}) \rho(\mathbf{y})}{|\mathbf{x} - \mathbf{y}|} \mathrm{d}x \mathrm{d}y \\
&- \sum_{K=1}^{M} \int_{\mathbb{R}^3} \frac{\rho(\boldsymbol{r})}{|\boldsymbol{r} - \boldsymbol{R}_K|} \mathrm{d}r + \frac{1}{2} \sum_{\mathbf{x} \neq \mathbf{y}} \frac{ce^2}{|\mathbf{x} - \mathbf{y}|},
\end{aligned}
\tag{108}
$$

and $\rho = \rho(r_1, r_2, r_3)$ is the electron density. Ritz Galerkin approximations of K and ρ yield approximations to E_{elec} in the same spirit as the Hartree-Fock example. The analysis then proceeds as in the Hartree-Fock cases.

A Posteriori Error Estimates. Estimation of the error, $E_{\text{elec}} - E_{\text{elec}}^h$ is an exercise in error estimation for nonlinear eigenvalue problems. The linear case is dealt with in [35]; the nonlinear case is open, but may be readily resolvable using ideas in [32].

8   Concluding Comments

That mathematical models of physical events are almost always imperfect abstractions of nature is a truism universally understood by all students of science and engineering. The possibility of quantifying in some way the level of imperfection is therefore an intriguing proposition. Our approach is to measure this imperfection as estimates of error in specific quantities that we single out as important features of the behavior of the system under consideration. But even then we do not escape the necessity of using another imperfect model, the base model of the event. Nevertheless, we believe that the relatively straightforward machinery we describe for comparing models by estimating modeling error can be very valuable, particularly when two or more models of events that occur at different scales are considered. If this process can be tied to physical measurements as well, it may be possible to develop powerful techniques for simulating events at multiple scales with a level of reliability beyond that thought possible in recent times.

There are many open issues that remain to be resolved. Given a list of quantities of interest for a base model at the finest scale, a systematic approach for developing the optimal ensemble-averaged or homogenized characterizations of these quantities at coarser scales is needed. We have offered some examples in this work, but further work

on how these averaging techniques affect accuracy of estimates and convergence rates of the adaptive process is needed.

Adaptive modeling techniques are in early stages of development. The Global- and Local-Goals algorithms presented here represent only two of many possible approaches. Other techniques could be inspired by many of the multigrid methods in use in linear and nonlinear solvers. The role of various hand-shake methods for interfacing models of different scales as a basis for adaptive modeling is also a topic worthy of further study.

There is also the issue of modifying the definition of a quantity of interest as one progresses to coarser-scale models. In a two-scale situation, the coarse-scale model is a surrogate: an artifact of a computational process. In more general situations, it can be conceived that coarser-scale models may possess features of interest themselves, not always tied to fine-scale quantities of interest. The procedures we developed here should be applicable to such situations with straightforward modifications. Of overriding importance is the goal of estimating the relative error in quantities delivered by two or more models.

Much work remains to be done on the QM-MD interface and on traversing hierarchies of QM-electronic models as well. We hope to explore some of these issues in future work.

References

[1] M. Ainsworth and J. T. Oden. *A Posteriori Error Estimation in Finite Element Analysis*. John Wiley & Sons, New York, 2000.

[2] Altair Engineering, Inc., Austin, Texas. *ProPHLEX User Manual Version 3.0*, 2000.

[3] W. Bangerth. A framework for the adaptive finite element solution of large inverse problems. I. Basic techniques. ICES Report 04-39, The University of Texas at Austin, 2004.

[4] W. Bangerth and R. Rannacher. *Adaptive Finite Element Methods for Solving Differential Equations*. Birkhäuser Verlag, 2003.

[5] R. Becker and R. Rannacher. An optimal control approach to a posteriori error estimation in finite element methods. *Acta Numerica*, 10:1–102, 2001.

[6] R. Becker and B. Vexler. Mesh refinement and numerical sensitivity analysis for parameter calibration of partial differential equations. *Journal of Computational Physics*, 206:95–110, 2005.

[7] T. Belytschko and S. P. Xiao. Coupling methods for continuum model with molecular model. *International Journal for Multiscale Computational Engineering*, 1(1):115–126, 2003.

[8] X. Blanc, C. L. Bris, and P. L. Lions. From molecular models to continuum mechanics. *Archives for Rational Mechanics and Analysis*, 164:341–381, 2002.

[9] M. Born. *Atomic Physics*. London, Blackie & son limited, 1935.

[10] J. Q. Broughton, F. F. Abraham, N. Bernstein, and E. Kaxiras. Concurrent coupling of length scales: Methodology and application. *Physical Review B*, 60(4):2391–2403, 1999.

[11] W. A. Curtin and R. E. Miller. Atomistic/continuum coupling in computational materials science. *Modelling Simul. Mater. Sci. Eng.*, 11:R33–R68, 2003.

[12] M. S. Daw and M. I. Baskes. Embedded-atom method: Derivation and applications to impurities, surfaces, and other defects in metals. *Physical Review B*, 29(12):6443–6453, 1984.

[13] W. E and B. Engquist. The heterogeneous multiscale methods. *Comm. Math. Sci.*, 1(1):87–132, 2003.

[14] W. E, B. Engquist, X. Li, W. Ren, and E. Vanden-Eijnden. The heterogeneous multiscale method: A review. Preprint, Princeton University, 2004. *Available at http://www.math.princeton.edu/multiscale/.*

[15] W. E, X. Li, and E. Vanden-Eijnden. Some recent progress in multiscale modeling. Preprint, Princeton University, 2004. *http://www.math.princeton.edu/multiscale/.*

[16] W. E, P. B. Ming, and P. W. Zhang. Analysis of the heterogeneous multiscale method for elliptic homogenization problems. *J. Amer. Math. Soc.*, 2004. To appear.

[17] V. Fock. Naherungsmethode zur lösung des quanten mechanischen mehrkörper-problemen. *Z. Phys.*, 61:126–148, 1930.

[18] S. M. Foiles, M. I. Baskes, and M. S. Daw. Embedded-atom-method functions for fcc metals Cu, Ag, Au, Ni, Pd, Pt, and their alloys. *Physical Review B*, 33(12):7983–7991, 1986.

[19] G. Friesecke and R. D. James. A scheme for passage from atomic to continuum theory for thin films, nanotubes, and nanorods. *J. Mechanics and Physics of Solids*, 48:1519–1540, 2000.

[20] G. Friesecke and F. Theil. Validity and failure of the cauchy-born hypothesis in a two-dimensional mass-spring lattice. *J. Nonlinear Sci.*, 12:445–478, 2002.

[21] D. Hartree. The wave mechanics of an atom with non-Coulomb central field, Part 1, Theory & Method. *Proc. Comb. Phil. Soc.*, 24:89–312, 1928.

[22] Z. Hashin. Analysis of composite materials, a survey. *J. Appl. Mech.*, 50:481–505, 1983.

[23] T. J. R. Hughes, G. R. Feijóo, L. Mazzei, and J.-B. Quincy. The variational multiscale method — a paradigm for computational mechanics. *Comput. Methods Appl. Mech. Engrg.*, 166:3–24, 1998.

[24] H. Johansson and K. Runesson. Parameter identification in constitutive models via optimization with a posteriori error control. *Int. J. Num. Meth. Engng.*, 62:1315–1340, 2005.

[25] S. Kohlhoff, P. Gumbsch, and H. F. Fischmeister. Crack propagation in b.c.c. crystals studied with a combined finite-element and atomistic model. *Phil. Mag. A*, 64(4):851–878, 1991.

[26] W. K. Liu, E. G. Karpov, S. Zhang, and H. S. Park. An introduction to computational nanomechanics and materials. *Comput. Methods Appl. Mech. Engng.*, 193:1529–1578, 2004.

[27] R. Miller, M. Ortiz, R. Phillips, V. Shenoy, and E. B. Tadmor. Quasicontinuum models of fracture and plasticity. *Eng. Fracture Mech.*, 61:427–444, 1998.

[28] R. E. Miller and E. B. Tadmor. The quasicontinuum method: Overview, applications, and current directions. *Journal of Computer-Aided Design*, 9:203–239, 2002.

[29] R. E. Miller and E. B. Tadmor. *QC Tutorial Guide Version 1.1*, May 2004. Available at www.qcmethod.com.

[30] R. E. Miller, E. B. Tadmor, R. Phillips, and M. Ortiz. Quasicontinuum simulation of fracture at the atomic scale. *Modeling Simul. Mater. Sci. Eng.*, 6:607–638, 1998.

[31] J. T. Oden and S. Prudhomme. Goal-oriented error estimation and adaptivity for the finite element method. *Computers and Mathematics with Applications*, 41:735–756, 2001.

[32] J. T. Oden and S. Prudhomme. Estimation of modeling error in computational mechanics. *Journal of Computational Physics*, 182:496–515, 2002.

[33] J. T. Oden, S. Prudhomme, and P. Bauman. On the extension of goal-oriented error estimation and hierarchical modeling to discrete lattice models. *Comput. Methods Appl. Mech. Engrg.*, 2005. In print.

[34] J. T. Oden, S. Prudhomme, A. Romkes, and P. Bauman. Multi-scale modeling of physical phenomena: Adaptive control of models. ICES Report 05-13, The University of Texas at Austin, 2005.

[35] J. T. Oden, S. Prudhomme, T. Westermann, J. Bass, and M. E. Botkin. Error estimation of eigenfrequencies for elasticity and shell problems. *Mathematical Models and Methods in Applied Sciences*, 13:323–344, 2003.

[36] J. T. Oden and K. Vemaganti. Estimation of local modeling error and goal-oriented modeling of heterogeneous materials; part I. Error estimates and adaptive algorithms. *Journal of Computational Physics*, 164:22–47, 2000.

[37] J. T. Oden, K. Vemaganti, and N. Moës. Hierarchical modeling of heterogeneous solids. *Comput. Methods Appl. Mech. Engng.*, 172:3–25, 1999.

[38] J. T. Oden and T. I. Zohdi. Analysis and adaptive modeling of highly heterogeneous elastic structures. *Comput. Methods Appl. Mech. Engng.*, 148:367–391, 1997.

[39] H. S. Park, E. G. Karpov, P. A. Klein, and W. K. Liu. Three-dimensional bridging scale analysis of dynamic fracture. Preprint.

[40] H. S. Park, E. G. Karpov, W. K. Liu, and P. A. Klein. The bridging scale for two dimensional atomistic/continuum coupling. *Philosiphical Magazine*, 85(1):79–113, 2005.

[41] R. Phillips, D. Rodney, V. Shenoy, E. B. Tadmor, and M. Ortiz. Hierarchical models of plasticity: dislocation nucleation and interaction. *Modeling Simul. Mater. Sci. Eng.*, 7:769–780, 1999.

[42] S. Prudhomme, P. Bauman, and J. T. Oden. Error control for molecular statics problems. In Preparation.

[43] D. Qian, G. J. Wagner, and W. K. Liu. A multiscale projection method for the analysis of carbon nanotubes. *Comput. Methods Appl. Mech. Engng.*, 193:1603–1632, 2004.

[44] D. Raabe. *Computational Materials Science: The Simulation of Materials Microstructures and Properties.* Wiley-VCH, Weinheim, 1998.

[45] A. Romkes and J. T. Oden. Adaptive modeling of wave propagation in heterogeneous elastic solids. *Comput. Methods Appl. Mech. Engng.*, 193:539–559, 2004.

[46] A. Romkes, J. T. Oden, and K. Vemaganti. Multi-scale goal-oriented adaptive modeling of random heterogeneous materials. *J. Mech. Mater.*, 2005. To appear.

[47] A. Romkes, K. Vemaganti, and J. T. Oden. The extension of the GOALS algorithm to the analysis of elastostatics problems of random heterogeneous materials. ICES Report 04-45, The University of Texas at Austin, 2004.

[48] V. B. Shenoy, R. Miller, E. B. Tadmor, R. Phillips, and M. Ortiz. Quasicontinuum models of interfacial structure and deformation. *Physical Review Letters*, 80:742–745, 1998.

[49] V. B. Shenoy, R. Miller, E. B. Tadmor, D. Rodney, R. Phillips, and M. Ortiz. An adaptive finite element approach to atomic-scale mechanics — the quasicontinuum method. *Journal of the Mechanics and Physics of Solids*, 47:611–642, 1999.

[50] L. E. Shilkrot, R. E. Miller, and W. A. Curtin. Coupled atomistic and discrete dislocation plasticity. *Physical Review Letters*, 89(2):025501–1–025501–4, 2002.

[51] L. E. Shilkrot, R. E. Miller, and W. A. Curtin. Multiscale plasticity modeling: Coupled atomistics and discrete dislocation mechanics. *Journal of the Mechanics and Physics of Solids*, 52:755–787, 2004.

[52] G. S. Smith, E. B. Tadmor, N. Bernstein, and E. Kaxiras. Multiscale simulations of silicon nanoindentation. *Acta. Mater.*, 49:4089–4101, 2001.

[53] E. B. Tadmor. *The Quasicontinuum Method.* PhD thesis, Brown University, 1996.

[54] E. B. Tadmor, R. Miller, R. Phillips, and M. Ortiz. Nanoindentation and incipient plasticity. *J. Mater. Res.*, 14:2233–2250, 1999.

[55] E. B. Tadmor, M. Ortiz, and R. Phillips. Quasicontinuum analysis of defects in solids. *Phil. Mag. A*, 73(6):1529–1563, 1996.

[56] S. Tang, T. Y. Hou, and W. K. L. Liu. A mathematical framework of the bridging scale method. In preparation.

[57] S. Tang, T. Y. Hou, and W. K. L. Liu. Pseudo-spectral multiscale method: Interfacial conditions and coarse grid equations. In preparation.

[58] E. van der Giessen and A. Needleman. Discrete dislocation plasticity: a simple planar model. *Modelling Simul. Mater. Sci. Eng.*, 3:689–735, 1995.

[59] K. Vemaganti and J. T. Oden. Estimation of local modeling error and goal-oriented modeling of heterogeneous materials; part II: A computational environment for adaptive modeling of heterogeneous elastic solids. *Comput. Meth. Appl. Mech. Engrg.*, 190:6089–6124, 2001.

[60] G. J. Wagner and W. K. Liu. Coupling of atomistic and continuum simulations using a bridging scale decomposition. *Journal of Computational Physics*, 190:249–274, 2003.

[61] S. P. Xiao and T. Belytschko. A bridging domain method for coupling continua with molecular dynamics. *Comput. Methods Appl. Mech. Engng.*, 193:1645–1669, 2004.

[62] O. C. Zienkiewicz and J. Z. Zhu. A simple error estimator and adaptive procedure for practical engineering analysis. *Int. J. Num. Meth. Engng.*, 24(2):337–357, 1987.

[63] T. I. Zohdi, J. T. Oden, and G. J. Rodin. Hierarchical modeling of heterogeneous bodies. *Comput. Methods Appl. Mech. Engng.*, 138:273–298, 1996.